

Interactive comment on “Significant wintertime PM_{2.5} mitigation in the Yangtze River Delta, China from 2016 to 2019: observational constraints on anthropogenic emission controls” by Liqiang Wang et al.

5

Anonymous Referee #1

Received and published: 20 August 2020

General comments:

10 Wang et al. evaluated the effect of long-term and emergent emission control strategies on the PM_{2.5} levels in Yangtze River Delta of China, by combining modelling analysis with observations. They found the decline in PM_{2.5} concentration during 2016-2019 was mainly due to emission control. The decline would be even greater if the meteorology was not unfavorable. Great potential of further decrease is manifested in analysis of data during G20 period when short-term emergent measures were taken. The discussion is valuable for assessment of past policies and design of future ones. However, to be publishable
15 in ACP, the current manuscript requires further improvement.

Response: We thank the reviewer for the thoughtful comments on our paper and have addressed them as below.

1. Particularly, inadequate credits are given to the existing literature that performed similar analysis of separating meteorology and emission effects on recent PM_{2.5} trend in China. Instead, the authors tried to impress the reader by suggesting that this
20 study is the first to do so. Just to list a few studies in literature (and I believe there might be more), Zhang et al., 2019. Drivers of improved PM_{2.5} air quality in China from 2013 to 2017, PNAS; Zhai et al., 2019. Fine particulate matter (PM_{2.5}) trends in China, 2013–2018: separating contributions from anthropogenic emissions and meteorology, ACP; Zhong et al., 2018. Distinguishing Emission-Associated Ambient Air PM_{2.5} Concentrations and Meteorological Factor-Induced Fluctuations, EST. The authors should review the existing literature and put emphasize on their innovations.

25 **Response:** We thank the reviewer for the valuable suggestions on the introduction. We have supplemented the additional discussions to introduce more literature, including all of the above works as well as someone else, in order to substantiate and improve the “Introduction”.

Added/rewritten part in Sect. 1: The main challenge involves reliably representing substantial and rapid changes in anthropogenic emissions resulting from both long-term and emergency control measures (Chen et al., 2019; Cheng et al., 2019;
30 Zhang et al., 2014; Yang et al., 2016; Zhai et al., 2019; Zhang et al., 2019; Zhong et al., 2018). To gain timely insight into variations in anthropogenic emissions, considerable efforts went into establishing detailed bottom-up emissions and derived valuable findings (Cheng et al., 2019; Zhang et al., 2019). Yet bottom-up inventories were built on the basis of activity data

and emission factors. These input data can be absent or outdated, likely leading to misunderstandings of anthropogenic impacts, particularly in terms of the magnitude (Jiang et al., 2018). Recent studies applied available observations to construct multilinear regression models (emission-based or meteorology-related), allowing us to separate contributions from anthropogenic emissions and meteorology to some extent (Zhai et al., 2019; Zhong et al., 2018). However, the uncertainties in bottom-up inventories and meteorological fields remained. Here we switched to observational constraints on a state-of-the-art chemical model. This can be a potential way to tackle this challenge.

2. I also have concerns about the methodology. Assimilation is used for calculating the total effect (emis+met) which gives a good representation of PM_{2.5} distributions, despite any model errors. But assimilation cannot be used for calculating met-only effect. Therefore, model errors may propagate into the met effect. I wonder what uncertainties this inconsistency in two pairs of simulations would cause for the results. The authors evaluated model emissions and concluded the impact is small. But it is not shown if other model errors may be significant. For example, studies have found that model tends to underestimate sulfate production during high RH in China. More evaluation of the model performance may be useful for interpreting the result.

Response: Thanks. Yes, we agree with the reviewer that more detailed model evaluation might be useful for this study. As previous studies have demonstrated (Cheng et al., 2019; Zhai et al., 2019; Zhong et al., 2018), model uncertainties remain, although we have verified the constrained results. We have supplemented the additional discussions in Sect. 4 for further explanations. For instance, model simulations of aerosol components (e.g., sulfate and nitrate) are still poorly constrained. Moreover, they have not been evaluated due to lack of available observations. Previous studies find that the model tends to underestimate sulfate production during high RH (as pointed by the reviewer) as well as SOA (Li et al., 2017a; Wang et al., 2014; Zhong et al., 2018). As a result, these uncertainties can be propagated into the estimations of meteorological effects. In addition, like other atmospheric chemical transport models, the WRF-CMAQ model cannot provide model uncertainty information in the simulations, while Monte Carlo simulations for complex CTMs would be unrealistic due to extremely high computation loadings (Zhong et al., 2018). Looking forward, more detailed model evaluations, as well as more explicit observational constraints, are of great significance for improving associated understandings, which will be the topic of a next separate study.

Added/rewritten part in Sect. 4: Note that, as previous studies have demonstrated (Cheng et al., 2019; Zhai et al., 2019; Zhong et al., 2018), model uncertainties remain, although we have verified the constrained results. We have supplemented the additional discussions in Sect. 4 for further explanation. For instance, model simulations of aerosol components (e.g., sulfate and nitrate) are still poorly constrained. Moreover, they have not been evaluated due to lack of available observations. Yet previous studies find that the model tends to underestimate sulfate production during high RH and SOA (Li et al., 2017a; Wang et al., 2014; Zhong et al., 2018). As a result, these uncertainties can be propagated into the estimations of meteorological effects. Besides, like other atmospheric chemical transport models, the WRF-CMAQ model cannot provide model uncertainty information in the simulations, while Monte Carlo simulations for complex CTMs would be unrealistic due to extremely high computation loadings (Zhong et al., 2018).

3. The inclusion of short-term G20 period is interesting. But I am not completely convinced that the mitigation potential map is useful at all. At a first glance, the map does not seem to be very different from conducting a zero-ish YRD emission simulation with the model and then do a subtraction. The problem is that the authors did not provide information about (1) what types or fractions of emissions were shut down during the event; (2) is the emission shutdown implemented in Hangzhou, or Zhejiang, or YRD? Without this information, it is not possible to interpret the mitigation potential.

Response: Thanks. We have supplemented the information associated with anthropogenic emission control measures during the G20 summit. On that occasion, anthropogenic emission controls were conducted across the whole YRD (including Zhejiang, Jiangsu, and Anhui provinces, and Shanghai municipality), particularly in Hangzhou that served as the host city (Li et al., 2019, 2017b; Ni et al., 2020; Yu et al., 2018). Li et al. (2017) showed that most of anthropogenic emissions (e.g., those from industry, power plant, residential, and on-road transportation sectors) were reduced by around 50% on the basis of available governmental information.

Added/rewritten part in Sect. 1: Those measures were conducted across the whole YRD (including Zhejiang, Jiangsu, and Anhui provinces, and Shanghai municipality), particularly in Hangzhou that served as the host city (Li et al., 2019, 2017b; Ni et al., 2020; Yu et al., 2018). Li et al. (2017) showed that most of anthropogenic emissions (e.g., those from industry, power plant, residential, and on-road transportation sectors) were reduced by around 50% on the basis of available governmental information.

Specific comments:

1. Line 41: Not clear from the text whether “> 14 $\mu\text{g}/\text{m}^3$, 19%” is $\text{PM}_{2.5}$ levels, or in fact, reduction in $\text{PM}_{2.5}$ concentrations. Please clarify.

Response: Thanks. We have deleted the numbers. Specific numbers have been given in the following part of “Abstract”.

2. Line 42-44: Confusing, as it interrupts the flow and misleads a reader that the decline in Hangzhou ($35 \mu\text{g}/\text{m}^3$) is due to G20 control measures. I suggest moving the sentence to either Line 40 after “YRD, China” or to Line 48 before “Compared to the long-term policies...”.

Response: Thanks. We suggest not to move this sentence. It follows behind the statement “For the winter time periods from 2016 to 2019” and is thus linked with the effects of the long-term policies from 2016 to 2019.

95

3. Line 46: remove “thus”

Response: Thanks. We have removed the word.

4. Line 99: should -> can

Response: Thanks. We have revised the word accordingly.

100

5. Line 105: "unprecedented" is a too-big word here that I suggest to remove. Same for other occurrences of the word in the paper.

Response: Thanks. We have removed the word throughout the paper.

105 6. Line 125: Be consistent with the citation format.

Response: Thanks. We have revised the format.

7. Line 137-139: Are meteorological observations assimilated in addition to chemical observations? If so, describe the meteorological observations that are assimilated. If not, I don't think it is sufficient to just use initial and boundary conditions
110 from reanalysis data. The WRF should be run in a nudging mode, so the meteorology is close to reality.

Response: Thanks. Yes, the ECMWF reanalysis datasets were used to constrain meteorological simulations. Therein almost all necessary meteorological factors (nine variables), involving temperature, U wind component, V wind component, pressure, relative humidity, precipitation, short-wave radiation, cloud cover, and planetary boundary layer height (PBLH), were assimilated (<https://apps.ecmwf.int/datasets/data/interim-full-daily/levtype=sfc/>, last access: 7 March 2020).

115 **Added/rewritten part in Sect. 2.4:** The ECMWF reanalysis datasets accounted for the hourly observational constraints on spatiotemporal meteorological evolutions. Therein almost all necessary meteorological factors (9 variables), involving temperature, U wind component, V wind component, pressure, relative humidity, precipitation, short-wave radiation, cloud cover, and planetary boundary layer height (PBLH), were assimilated (<https://apps.ecmwf.int/datasets/data/interim-full-daily/levtype=sfc/>, last access: 7 March 2020).

120

8. Line 155: "Prior anthropogenic emissions"? Do you optimize emissions at all? I cannot find such description throughout the text. If not, it should not be called "prior".

Response: Thanks. We have revised the word accordingly.

125 9. Line 166: "more" is not a proper conjunction word in formal English writing.

Response: Thanks. We have revised the word to "Moreover".

10. Line 176: grids -> grid cells

Response: Thanks. We have revised the word accordingly.

130

11. Line 176: "potential excellent roles" Rephrase it.

Response: Thanks. We have revised the phrase to "potentially excellent roles".

12. Section 2.4: What is the assimilation window? Daily? hourly?

- 135 **Response:** Thanks. The assimilation window is hourly. We have highlighted this in the Sect. 2.4.
Added/rewritten part in Sect. 2.4: When ground-level PM_{2.5} measurements were assimilated, hourly observations were put into equation (1) to construct the new analysis fields. All-day state variables associated with aerosols in the model were adjusted from their background (simulated) to their analysis (constrained) states using the scaling factors (X^a/X^b).
- 140 13. Line 212: “the threshold pinpointing the key value of the correlation coefficients (e^{-1})”. -> e-folding length
Response: Thanks. We have revised the sentence.
Added/rewritten part in Sect. 2.3: The results indicated that a correlation length scale of ~ 180 km could be treated as the threshold. It allowed the correlation coefficients to fall within the range of e^{-1} , defining the effective radius of each individual observation.
- 145 14. Line 217-219: well, it is still static in the relative sense. I don’t this means anything. I’d suggest removing this statement.
Response: Thanks. We have removed the sentence.
15. Line 231: “unify the chemical inputs for the WRF-CMAQ model”. What does this mean?
150 **Response:** Thanks. We have revised the sentence to further clarify the meaning.
Added/rewritten part in Sect. 2.4: These configurations unified both chemical (i.e., emission inventories) and meteorological input data for the WRF-CMAQ model.
16. Line 237-240: Up to this point, we still do not know what method the authors use to separate effects of meteorology and
155 emission. A clear description of the method is needed before this point.
Response: Thanks. We have revised the sentence to further clarify the meaning.
Added/rewritten part in Sect. 2.4: Specifically, the differences in the constrained PM_{2.5} concentrations between DA_2016 and DA_2019 reflected the net effects of anthropogenic emission controls and meteorological perturbations between 2016 and 2019, while meteorological impacts therein were calculated as the differences in simulated PM_{2.5} concentrations between
160 NO_2016 and NO_2019 (Chen et al., 2019a). Hence, by subtracting meteorological impacts from the net effects, we can isolate the effects of anthropogenic emission controls attributable to the long-term strategies.
17. Line 257: It is cursory to conclude these three periods have similar meteorology based on Fig. S1. The validity of the
analysis is relied on the assumption that they are similar. E.g., one factor that is not analyzed is wind direction. Showing maps
165 of circulation pattern will also help.
Response: Thanks. We have supplemented the map of atmospheric synoptic circulation patterns in Figure S1 accordingly (Dong et al., 2020; Liu et al., 2019).

170 18. Fig. 4. Is Fig. 4 useful? It is no surprising that the assimilated simulation could better reproduce observations, which are used in assimilation. It means nothing.

Response: Thanks. This figure is used to verify whether the model coupled with the OI method could reproduce the measurements. While 244 monitoring stations reside in 6660 grid cells, 16 grid cells have two to three monitors in them. For these grid cells, only one averaged measurement was used for DA. However, all the observations were compared against the constrained results. Hence, we suggest not to remove the figure and have supplemented the additional discussions in the Sect.

175 2.4.

Added/rewritten part in Sect. 2.4: While 244 monitoring stations reside in 6660 grid cells, 16 grid cells have two to three monitors in them. For these grid cells, only one averaged measurement was used for DA. However, all the observations were compared against the constrained results in the analyses.

180 19. Line 307-311. There is a jump in the logic of this sentence. I'd remove it.

Response: Thanks. We have removed the sentence.

20. Line 350-352: Many studies have properly separated the effects from meteorology and emissions, though with different approaches. I don't think the statement is fair.

185 **Response:** Thanks. We have revised the sentence.

Added/rewritten part in Sect. 3.2: This also indirectly implied the importance of assimilating meteorology, which, however, were generally neglected by previous studies (Chen et al., 2019).

190 21. Line 353: It's unclear to me whether 5% and 3% are relative to mean $PM_{2.5}$ concentration or mean reduction of $PM_{2.5}$. Be more explicit.

Response: Thanks. We have added the absolute concentrations to make it clear.

Added/rewritten part in Sect. 3.2: As shown in Figure S10 and Figure 5, even with the largest adjustment (i.e., -40%), such interferences could be well controlled within the 5% ($< 3 \mu\text{g}/\text{m}^3$) scope, let alone other tests (i.e., $< 3\%$, $< 2 \mu\text{g}/\text{m}^3$).

195 22. Line 355: how do you prove it was "under the same meteorological condition".

Response: Thanks. We have revised the sentence to further clarify the meaning.

Added/rewritten part in Sect. 3.2: Moreover, these findings are consistent with previous analyses (Cheng et al., 2019; Zhang et al., 2019). They generally revealed that reasonable changes in the bottom-up emissions, together with the same meteorology input data, would not remarkably alter the simulated results associated with meteorological effects on surface $PM_{2.5}$ ($< 5\%$).

200

23. Line 370: what is "concurrent meteorology"? better to rephrase it.

Response: Thanks. We have revised the phrase to "meteorological conditions therein".

24. Line 375-376: Of course, the long-term strategies are emission oriented. You cannot change weather easily after all ... I
205 guess the author wanted to say the long-term decrease in PM_{2.5} was driven mainly by decreased emissions.

Response: Thanks. We agree. We have revised the sentence.

Added/rewritten part in Sect. 3.2: This indicates that the impacts of the long-term strategies are mainly driven by anthropogenic emission mitigation.

210 25. Line 387: what is “stably spatiotemporal state”. Rephrase it.

Response: Thanks. We have revised the sentence.

Added/rewritten part in Sect. 3.3: We found that such impacts were of relatively low standard deviations (< 5%) and kept stable over time.

215 26. Line 412: remove “unprecedented”.

Response: Thanks. We have removed the word throughout the paper.

27. Line 414: what is “stable supply-side structures”? Not directly related to air quality to me.

Response: Thanks. We have revised the phrase to “stable structures of anthropogenic emissions”.

220

28. Line 418: There have been quite a few papers discussing the effect of emission control strategy. To list a few, Zhang et al.,
2019. Drivers of improved PM_{2.5} air quality in China from 2013 to 2017, PNAS Zhai et al., 2019. Fine particulate matter
(PM_{2.5}) trends in China, 2013–2018: separating contributions from anthropogenic emissions and meteorology, ACP Zhong et
al., 2018. Distinguishing Emission-Associated Ambient Air PM_{2.5} Concentrations and Meteorological Factor-Induced
225 Fluctuations, EST Although the method may not be the same, the authors should give credit to these studies rather than claim
this is the first study trying to separate effects of met and emission.

Response: Thanks. We have addressed this issue in the response for the general comment (1). We have supplemented the additional discussions to introduce more literature, including all of the above works as well as someone else, in order to substantiate and improve the “Introduction”.

230 **Added/rewritten part in Sect. 1:** The main challenge involves reliably representing substantial and rapid changes in anthropogenic emissions resulting from both long-term and emergency control measures (Chen et al., 2019; Cheng et al., 2019; Zhang et al., 2014; Yang et al., 2016; Zhai et al., 2019; Zhang et al., 2019; Zhong et al., 2018). To gain timely insight into variations in anthropogenic emissions, considerable efforts went into establishing detailed bottom-up emissions and derived valuable findings (Cheng et al., 2019; Zhang et al., 2019). Yet bottom-up inventories were built on the basis of activity data
235 and emission factors. These input data can be absent or outdated, likely leading to misunderstandings of anthropogenic impacts, particularly in terms of the magnitude (Jiang et al., 2018). Recent studies applied available observations to construct multilinear

240 regression models (emission-based or meteorology-related), allowing us to separate contributions from anthropogenic emissions and meteorology to some extent (Zhai et al., 2019; Zhong et al., 2018). However, the uncertainties in bottom-up inventories and meteorological fields remained. Here we switched to observational constraints on a state-of-the-art chemical model. This can be a potential way to tackle this challenge.

29. Line 444: "rudimentary" may not be a proper word here.

Response: Thanks. We have removed the word.

245

30. Line 449: the statement that “the biogenic emissions are unimportant for IAV of PM_{2.5}” may be true for YRD, but may not be “generally” true for elsewhere in the world. I’d suggest being more specific.

Response: Thanks. We have revised the sentence to make it more specific.

250 **Added/rewritten part in Sect. 4:** Moreover, the former is generally of minor significance for interannual PM_{2.5} variations for the YRD.

References:

- Chen, D., Liu, Z., Ban, J., Zhao, P. and Chen, M.: Retrospective analysis of 2015--2017 wintertime PM 2.5 in China: response to emission regulations and the role of meteorology, *Atmos. Chem. Phys.*, 19(11), 7409–7427, 2019a.
- 255 Chen, D., Liu, Z., Ban, J., Zhao, P. and Chen, M.: Retrospective analysis of 2015-2017 wintertime PM_{2.5} in China: response to emission regulations and the role of meteorology, *Atmos. Chem. Phys.*, 19(11), 7409–7427, 2019b.
- Chen, D., Liu, Z., Ban, J. and Chen, M.: The 2015 and 2016 wintertime air pollution in China: SO₂ emission changes derived from a WRF-Chem/EnKF coupled data assimilation system, *Atmos. Chem. Phys.*, 19(13), 8619–8650, 2019c.
- Cheng, J., Su, J., Cui, T., Li, X., Dong, X., Sun, F., Yang, Y., Tong, D., Zheng, Y., Li, Y. and others: Dominant role of
260 emission reduction in PM_{2.5} air quality improvement in Beijing during 2013--2017: A model-based decomposition analysis, *Atmos. Chem. Phys.*, 19(9), 6125–6146, 2019.
- Dong, Y., Li, J., Guo, J., Jiang, Z., Chu, Y., Chang, L., Yang, Y. and Liao, H.: The impact of synoptic patterns on summertime ozone pollution in the North China Plain, *Sci. Total Environ.*, 735, 139559, doi:<https://doi.org/10.1016/j.scitotenv.2020.139559>, 2020.
- 265 Jiang, Z., McDonald, B. C., Worden, H., Worden, J. R., Miyazaki, K., Qu, Z., Henze, D. K., Jones, D. B. A., Arellano, A. F., Fischer, E. V and others: Unexpected slowdown of US pollutant emission reduction in the past decade, *Proc. Natl. Acad. Sci.*, 115(20), 5099–5104, 2018.
- Li, G., Bei, N., Cao, J., Huang, R., Wu, J., Feng, T., Wang, Y., Liu, S., Zhang, Q., Tie, X. and Molina, L. T.: A possible pathway for rapid growth of sulfate during haze days in China, *Atmos. Chem. Phys.*, 17(5), 3301–3316, doi:10.5194/acp-17-
270 3301-2017, 2017a.

- Li, H., Wang, D., Cui, L., Gao, Y., Huo, J., Wang, X., Zhang, Z., Tan, Y., Huang, Y., Cao, J. and others: Characteristics of atmospheric PM_{2.5} composition during the implementation of stringent pollution control measures in Shanghai for the 2016 G20 summit, *Sci. Total Environ.*, 648, 1121–1129, 2019.
- 275 Li, P., Wang, L., Guo, P., Yu, S., Mehmood, K., Wang, S., Liu, W., Seinfeld, J. H., Zhang, Y., Wong, D. C. and others: High reduction of ozone and particulate matter during the 2016 G-20 summit in Hangzhou by forced emission controls of industry and traffic, *Environ. Chem. Lett.*, 15(4), 709–715, 2017.
- Liu, N., Zhou, S., Liu, C. and Guo, J.: Synoptic circulation pattern and boundary layer structure associated with PM_{2.5} during wintertime haze pollution episodes in Shanghai, *Atmos. Res.*, 228, 186–195, doi:<https://doi.org/10.1016/j.atmosres.2019.06.001>, 2019.
- 280 Ni, Z.-Z., Luo, K., Gao, Y., Gao, X., Jiang, F., Huang, C., Fan, J.-R., Fu, J. S. and Chen, C.-H.: Spatial--temporal variations and process analysis of O₃ pollution in Hangzhou during the G20 summit, *Atmos. Chem. Phys.*, 20(10), 5963–5976, doi:10.5194/acp-20-5963-2020, 2020.
- Wang, Y., Zhang, Q., Jiang, J., Zhou, W., Wang, B., He, K., Duan, F., Zhang, Q., Philip, S. and Xie, Y.: Enhanced sulfate formation during China's severe winter haze episode in January 2013 missing from current models, *J. Geophys. Res.* 285 *Atmos.*, 119(17), 10,410–425,440, doi:10.1002/2013JD021426, 2014.
- Yang, Y., Liao, H. and Lou, S.: Increase in winter haze over eastern China in recent decades: Roles of variations in meteorological parameters and anthropogenic emissions, *J. Geophys. Res. Atmos.*, 121(21), 13,13–50,65, doi:10.1002/2016JD025136, 2016.
- 290 Yu, H., Dai, W., Ren, L., Liu, D., Yan, X., Xiao, H., He, J. and Xu, H.: The effect of emission control on the submicron particulate matter size distribution in Hangzhou during the 2016 G20 Summit, *Aerosol Air Qual. Res.*, 18, 2038–2046, 2018.
- Zhai, S., Jacob, D. J., Wang, X., Shen, L., Li, K., Zhang, Y., Gui, K., Zhao, T. and Liao, H.: Fine particulate matter (PM_{2.5}) trends in China, 2013–2018: separating contributions from anthropogenic emissions and meteorology, *Atmos. Chem. Phys.*, 19(16), 11031–11041, doi:10.5194/acp-19-11031-2019, 2019.
- 295 Zhang, R., Li, Q. and Zhang, R.: Meteorological conditions for the persistent severe fog and haze event over eastern China in January 2013, *Sci. China Earth Sci.*, 57(1), 26–35, doi:10.1007/s11430-013-4774-3, 2014.
- Zhang, Q., Zheng, Y., Tong, D., Shao, M., Wang, S., Zhang, Y., Xu, X., Wang, J., He, H., Liu, W. and others: Drivers of improved PM_{2.5} air quality in China from 2013 to 2017, *Proc. Natl. Acad. Sci.*, 2019.
- 300 Zhong, Q., Ma, J., Shen, G., Shen, H., Zhu, X., Yun, X., Meng, W., Cheng, H., Liu, J., Li, B., Wang, X., Zeng, E. Y., Guan, D. and Tao, S.: Distinguishing emission-associated ambient air PM_{2.5} concentrations and meteorological factor-induced fluctuations, *Environ. Sci. Technol.*, 52(18), 10416–10425, doi:10.1021/acs.est.8b02685, 2018.

Interactive comment on “Significant wintertime PM_{2.5} mitigation in the Yangtze River Delta, China from 2016 to 2019: observational constraints on anthropogenic emission controls” by Liqiang Wang et al.

5

Anonymous Referee #2

General comments:

This paper uses a data assimilation method to constrain the modelled PM_{2.5} concentrations over the Yangtze River Delta (YRD) region and distinguish the impact on PM_{2.5} from meteorology and emission variations. The results show that the emission reduction measures in G20 summit and long-term emission control strategies in YRD successfully curb the PM_{2.5} levels both locally and regionally. This paper is good in general and within the scope of Atmospheric Chemistry and Physics. I recommend for publication once the specific comments expressed below are addressed.

Response: We thank the reviewer for the thoughtful comments on our paper and have addressed these specific comments as below.

15

Specific comments:

1. The author should provide more details regarding how to conduct data assimilation. First, the author needs to perform a sensitivity analysis in order to proof that choosing the fan-shaped quadrilateral (Figure 1a) minimizes the impact from outside on the YRD region. Second, how is the modelled PM_{2.5} constrained spatiotemporally by observations, applying DA generated scaling factors to the whole fan-shaped quadrilateral region, the YRD region, city by city, or grid by grid, and hour by hour or day by day?

Response: Thanks. We have supplemented the additional discussions in Sect. 2.3 to explain why we choose the ground-level observations within the fan-shaped quadrilateral to constrain the model performance. As pointed by the reviewer, we aim to minimize the impacts outside the YRD region. Specifically, this was mainly due to the fact that this fan-shaped geographical scope covered almost all key regions that had potentially regional impacts on the YRD, involving the Beijing-Tianjin-Hebei region (BTH), the Pearl River Delta region, the Sichuan-Chongqing region, and the Shaanxi-Gansu region (Zhang et al., 2019). On the other hand, the ground monitoring sites within the fan-shaped quadrilateral were significantly denser than those outside, thus leading to much more effective DA in practice (Bocquet et al., 2015; Chai et al., 2017). Therefore, to assimilate the observations within the fan-shaped quadrilateral might be a sensible way to balance the DA effectiveness and computing efficiency. A resultant evidence lies in the model performance evaluation in Sect. 3.1, which would prove that this DA

30

configuration can enable reliable PM_{2.5} simulations. Collectively, we might eliminate the need of the associated sensitivity analysis.

In addition, we have supplemented the more discussions in Sect. 2.4 to further detail how to conduct observational constraints on the model simulations spatiotemporally. In short, we conducted hourly DA for grid cells. Note that the effective radius of each individual observation should be calculated in advance. When ground-level PM_{2.5} measurements were assimilated, hourly observations were put into equation (1) to construct the new analysis fields. All-day state variables associated with aerosols in the model were adjusted from their background (simulated) to their analysis (constrained) states using the scaling factors ($\mathbf{X}^a/\mathbf{X}^b$). The adjusted model state variables were then used to initiate the model to predict the next background state (\mathbf{X}^b) in Equation (1). Therefore, the background state (\mathbf{X}^b) served as a prior model prediction before it was combined with the newly available observation (\mathbf{Y}) to generate a new analysis state (\mathbf{X}^a) using Equation (1).

Measurements within the background-error correlation length scale were used to shape analysis states (\mathbf{X}^a). The background error covariance \mathbf{COV}_{ij} between any two grid cells \mathbf{i} and \mathbf{j} was simulated as

$$\mathbf{COV}_{ij} = \boldsymbol{\varepsilon}_i \boldsymbol{\varepsilon}_j e^{-\frac{\Delta_{ij}}{L}} \quad (2)$$

where $\boldsymbol{\varepsilon}_i$ and $\boldsymbol{\varepsilon}_j$ referred to the standard deviations of the background errors in two grid cells and Δ_{ij} denoted the distance between the two grids. As a result, L was the background-error correlation length scale, which can be the Hollingsworth-Lönnerberg method (Chai et al., 2017; Hollingsworth and Lönnerberg, 1986; Kumar et al., 2012). Figure 2 shows the correlation coefficient, i.e., $\mathbf{COV}_{ij}/\boldsymbol{\varepsilon}_i \boldsymbol{\varepsilon}_j$, as a function of the separation distance between two grid cells, which was averaged over 10 km bins. The results indicate that a correlation length scale of ~ 180 km could be treated as the threshold by allowing the correlation coefficients to fall within the range of e^{-1} , defining the effective radius of each individual observation. Due to the intensive monitoring sites in our study domain, this threshold was applied uniformly for the YRD. In this study, observations beyond the background-error correlation length scale would have no effect on \mathbf{X}^a .

Added/rewritten part in Sect. 2.3: As shown in Figure 1a, to consider regional impacts outside the YRD, the ground-level observations in the fan-shaped quadrilateral were used to constrain the model performance. This was mainly due to the fact that this fan-shaped geographical scope covered almost all key regions that had potentially regional impacts on the YRD, involving the Beijing-Tianjin-Hebei region (BTH), the Pearl River Delta region, the Sichuan-Chongqing region, and the Shaanxi-Gansu region (Zhang et al., 2019). On the other hand, the ground monitoring sites within the fan-shaped quadrilateral were significantly denser than those outside, thus leading to much more effective DA results in practice (Bocquet et al., 2015; Chai et al., 2017). Collectively, to assimilate the observations in the fan-shaped quadrilateral might be a sensible way to balance the DA effectiveness and the computing efficiency. A resultant evidence lies in the model performance evaluation in Sect. 3.1, which would prove that this DA configuration can enable reliable PM_{2.5} simulations.

Added/rewritten part in Sect. 2.4: When ground-level PM_{2.5} measurements were assimilated, hourly observations were put into equation (1) to construct the new analysis fields. All-day state variables associated with aerosols in the model were adjusted from their background (simulated) to their analysis (constrained) states using the scaling factors ($\mathbf{X}^a/\mathbf{X}^b$). The

65 adjusted model state variables were then used to initiate the model to predict the next background state (\mathbf{X}^b) in equation (1).
Therefore, the background state (\mathbf{X}^b) served as a prior model prediction before it was combined with the newly available
observation (\mathbf{Y}) to generate a new analysis state (\mathbf{X}^a) using Equation (1).

Measurements within the background-error correlation length scale were used to shape analysis states (\mathbf{X}^a). The background
error covariance \mathbf{COV}_{ij} between any two grid cells \mathbf{i} and \mathbf{j} was simulated as

70
$$\mathbf{COV}_{ij} = \boldsymbol{\varepsilon}_i \boldsymbol{\varepsilon}_j e^{-\frac{\Delta_{ij}}{L}} \quad (2)$$

where $\boldsymbol{\varepsilon}_i$ and $\boldsymbol{\varepsilon}_j$ referred to the standard deviations of the background errors in two grid cells and Δ_{ij} denoted the distance
between the two grids. As a result, L was the background-error correlation length scale, which can be obtained by the
Hollingsworth-Lönnerberg method (Chai et al., 2017; Hollingsworth and Lönnerberg, 1986; Kumar et al., 2012). Figure 2 shows
the correlation coefficient, i.e., $\mathbf{COV}_{ij}/\boldsymbol{\varepsilon}_i \boldsymbol{\varepsilon}_j$, as a function of the separation distance between two grid cells, which was averaged
75 over 10 km bins. The results indicated that a correlation length scale of ~ 180 km could be treated as the threshold allowing
the correlation coefficients to fall within the range of e^{-1} , defining the effective radius of each individual observation. Due to
the intensive monitoring sites in our study domain, this threshold was applied uniformly for the YRD. In this study,
observations beyond the background-error correlation length scale were assumed to have no effect on \mathbf{X}^a .

80 2. The author used a statistical method to establish the correlation coefficients and chose separation distance of 180 km as a
threshold. The author needs to give more explanations on the value of chosen. If the purpose is to find a correlation length
scale to minimize the effect on \mathbf{X}^a , based on Fig 2, it seems that separation distance of 600 km would be more appropriate.

Response: Thanks. The objective of identifying the background-error correlation length scale is to define the effective radius
of each individual observation and thus to establish reliable analysis states (\mathbf{X}^a). Here the Hollingsworth-Lönnerberg approach,
85 wildly used for decades (Chai et al., 2017; Hollingsworth and Lönnerberg, 1986; Kumar et al., 2012), is applied to calculate the
background-error correlation length scale. Observations beyond the background-error correlation length scale were assumed
to have no effect on \mathbf{X}^a . Once observations far away are introduced, more background errors \mathbf{COV}_{ij} , larger than e^{-1} , would
be put into \mathbf{X}^a as calculated in Equation (2). Corresponding detailed information has been given in the response for the specific
comment (2).

90 3. How did the author isolate the impact from emission reductions on $\text{PM}_{2.5}$ concentrations? Did the author use the constrained
 $\text{PM}_{2.5}$ subtract the impact on simulated $\text{PM}_{2.5}$ from meteorological variations? Even the modelled temperature, humidity, wind
speed, and air pressure were also assimilated in this study, there are other parameters, for example, modelled PBL height,
causing large uncertainties in the modelled meteorological field, and thus leading to bias and error in the calculated net impacts
95 from emission variations. For example, figures c and f in Fig 5, show very small impact of anthropogenic emission control
from 2016 to 2019 in most of Zhejiang province compared to the other provinces in the YRD region. Is it reasonable?

Response: Thanks. Yes, it is reasonable. We isolated anthropogenic impacts on PM_{2.5} concentrations by subtracting the corresponding meteorological impacts from the constrained PM_{2.5} fields. To further illustrate the process of meteorological assimilations, we have supplemented the additional discussions in Sect. 2.4. The ECMWF reanalysis datasets accounted for the hourly observational constraints on spatiotemporal meteorological evolutions. Therein almost all necessary meteorological factors (nine variables), involving temperature, U wind component, V wind component, pressure, relative humidity, precipitation, short-wave radiation, cloud cover, and boundary layer height, were assimilated (<https://apps.ecmwf.int/datasets/data/interim-full-daily/levtype=sfc/>, last access: 7 March 2020).

The model evaluation provides a more direct way to verify the corresponding model performance. As highlighted in Sect. 3.1, given the fact that the assimilated ERA reanalysis dataset has much wider spatial coverage than ground-based measurements, we also reproduced the spatiotemporal variations in the meteorological factors (e.g., temperature, relative humidity, wind speed, and air pressure) (Figures S5 ~ S8). Together with the comprehensive evaluation statistics as summarized in Tables S1 ~ S5, it has been demonstrated that the DA method can enable one to derive not only reliable PM_{2.5} evolution but also accurate meteorological fields.

In terms of the issue associated with Zhejiang, we have supplemented the additional interpretations in Sect. 3.2. The impacts of anthropogenic drivers on PM_{2.5} concentrations in the southern and eastern parts of Zhejiang were evidently weaker than those in other regions in the YRD. This divergence can mostly be explained by spatial distributions of anthropogenic emissions. Anthropogenic emissions in the southern and eastern parts of Zhejiang were also significantly less than those in other regions (Figure S9), thus leading to substantially low PM_{2.5} concentrations (Figure 3). Besides, meteorological fields in the coastal regions, more conducive to PM_{2.5} diffusions (Figure 5), might be another cause.

Added/rewritten part in Sect. 2.4: For all experiments, the prior anthropogenic emissions were kept consistent (i.e., MEIC), while the ECMWF reanalysis datasets accounted for the hourly observational constraints on spatiotemporal meteorological evolutions. The ECMWF reanalysis datasets accounted for the hourly observational constraints on spatiotemporal meteorological evolutions. Therein almost all necessary meteorological factors (nine variables), involving temperature, U wind component, V wind component, pressure, relative humidity, precipitation, short-wave radiation, cloud cover, and planetary boundary layer height (PBLH), were assimilated (<https://apps.ecmwf.int/datasets/data/interim-full-daily/levtype=sfc/>, last access: 7 March 2020).

Added/rewritten part in Sect. 3.1: In addition, given the fact that the assimilated ERA reanalysis dataset has much wider spatial coverage than ground-based measurements, we also reproduced the spatiotemporal variations in the meteorological factors (e.g., temperature, relative humidity, wind speed, and air pressure) (Figures S5 ~ S8). With the comprehensive evaluation statistics as summarized in Tables S1 ~ S5, it has been demonstrated that the DA method can enable one to derive not only reliable PM_{2.5} evolutions but also accurate meteorological fields.

Added/rewritten part in Sect. 3.2: We recognized that the impacts of anthropogenic drivers on PM_{2.5} concentrations in the southern and eastern parts of Zhejiang were evidently weaker than those in other regions in the YRD. This divergence can mostly be explained by spatial distributions of anthropogenic emissions. Anthropogenic emissions in the southern and eastern

of Zhejiang were also significantly less than those in other regions (Figure S9), thus leading to substantially low PM_{2.5} concentrations (Figure 3). Besides, meteorological fields in the coastal regions, more conducive to PM_{2.5} diffusions (Figure 5), might be another cause.

135 4. How did the author consider the regional transport of PM_{2.5} in this study? The regional emission control effect on PM_{2.5} may have influence on calculated net impact of emission reduction in each city and the localized mitigation potential.

Response: Thanks. We agree with the reviewer that regional transport of PM_{2.5} is central to our results and thus have considered it carefully. Using observational constraints on the state-of-the-art model, we have reproduced spatiotemporal variations in both PM_{2.5} and meteorological factors, as illustrated in Sect. 3.1, and thus derived the reliable estimations of regional transport of PM_{2.5}. Hence, we have supplemented a sentence in Sect. 3.1 to highlight this point.

140 Considering the main objective of this work, we have not conducted source apportionments to predict the impacts of regional transport of PM_{2.5}. In theory, regional transport of PM_{2.5} can be attributable to both anthropogenic and meteorological drivers. In turn, we provide paired experiment designs to isolate anthropogenic impacts by subtracting meteorological perturbations (i.e., the differences in simulated PM_{2.5} concentrations between NO_2016 and NO_2019 and between DA_CON_G20 and
145 NO_CON_G20) from the constrained PM_{2.5} fields (i.e., DA_2016 and DA_2019 / DA_G20).

Added/rewritten part in Sect. 3.1: Regional transport of PM_{2.5} can thus be captured reasonably in this way.

References:

- Chai, T., Kim, H.-C., Pan, L., Lee, P. and Tong, D.: Impact of Moderate Resolution Imaging Spectroradiometer Aerosol
150 Optical Depth and AirNow PM_{2.5} assimilation on Community Multi-scale Air Quality aerosol predictions over the contiguous United States, *J. Geophys. Res. Atmos.*, 122(10), 5399–5415, 2017.
- Hollingsworth, A. and Lönnberg, P.: The statistical structure of short-range forecast errors as determined from radiosonde data. Part I: The wind field, *Tellus A*, 38(2), 111–136, 1986.
- Kumar, U., De Ridder, K., Lefebvre, W. and Janssen, S.: Data assimilation of surface air pollutants (O₃ and NO₂) in the
155 regional-scale air quality model AURORA, *Atmos. Environ.*, 60, 99–108,
doi:<https://doi.org/10.1016/j.atmosenv.2012.06.005>, 2012.
- Mehmood, K., Wu, Y., Wang, L., Yu, S., Li, P., Chen, X., Li, Z., Zhang, Y., Li, M., Liu, W., Wang, Y., Liu, Z., Zhu, Y.,
Rosenfeld, D. and Seinfeld, J. H.: Relative effects of open biomass burning and open crop straw burning on haze formation
over central and eastern China: modeling study driven by constrained emissions, *Atmos. Chem. Phys.*, 20(4), 2419–2443,
160 doi:[10.5194/acp-20-2419-2020](https://doi.org/10.5194/acp-20-2419-2020), 2020.
- Zhang, Q., Zheng, Y., Tong, D., Shao, M., Wang, S., Zhang, Y., Xu, X., Wang, J., He, H., Liu, W. and others: Drivers of improved PM_{2.5} air quality in China from 2013 to 2017, *Proc. Natl. Acad. Sci.*, 116, 24463–24469, 2019.

1 **Significant wintertime PM_{2.5} mitigation in the Yangtze River Delta,**
2 **China from 2016 to 2019: observational constraints on anthropogenic**
3 **emission controls**

4 Liqiang Wang¹, Shaocai Yu^{*1,2}, Pengfei Li^{*3,1}, Xue Chen¹, Zhen Li¹, Yibo Zhang¹, Mengying Li¹, Khalid
5 Mehmood¹, Weiping Liu¹, Tianfeng Chai⁴, Yannian Zhu⁵, Daniel Rosenfeld⁶, and John H. Seinfeld²
6

7 ¹Research Center for Air Pollution and Health; Key Laboratory of Environmental Remediation and Ecological Health, Ministry
8 of Education, College of Environment and Resource Sciences, Zhejiang University, Hangzhou, Zhejiang 310058, P.R. China

9 ²Division of Chemistry and Chemical Engineering, California Institute of Technology, Pasadena, CA 91125, USA

10 ³College of Science and Technology, Hebei Agricultural University, Baoding, Hebei 071000, P.R. China

11 ⁴Air Resources Laboratory, NOAA, Cooperative Institute for Satellite Earth System Studies (CISESS), University of Maryland,
12 College Park, USA

13 ⁵Meteorological Institute of Shanxi Province, 36 Beiguangzhengjie, Xi'an 710015, China

14 ⁶Institute of Earth Science, The Hebrew University of Jerusalem, Jerusalem, Israel

15

16 Correspondence to: Shaocai Yu (shaocaiyu@zju.edu.cn); Pengfei Li (lpf_zju@163.com)

17

18

19

20

To be submitted to

21

Atmospheric Chemistry and Physics

22

23

24

25

26 **ABSTRACT**

27 Ambient fine particulate matter (PM_{2.5}) mitigation relies strongly on anthropogenic emission control measures, the actual
28 effectiveness of which is challenging to pinpoint owing to the complex synergies between anthropogenic emissions and
29 meteorology. Here, observational constraints on model simulations allow us to derive not only reliable PM_{2.5} evolution but
30 also accurate meteorological fields. On this basis, we isolate meteorological factors to achieve reliable estimates of surface
31 PM_{2.5} responses to both long-term and emergency emission control measures from 2016 to 2019 over the Yangtze River Delta
32 (YRD), China. The results show that long-term emission control strategies play a crucial role in curbing PM_{2.5} levels, especially
33 in the megacities and other areas with abundant anthropogenic emissions. The G20 summit hosted in Hangzhou in 2016
34 provides a unique and ideal opportunity involving the most stringent, even unsustainable, emergency emission control
35 measures. The most substantial declines in PM_{2.5} concentrations ($\sim 35 \mu\text{g}/\text{m}^3$, $\sim 59\%$) are achieved in Hangzhou and its
36 surrounding areas. The following hotspots also emerge in megacities, especially in Shanghai ($32 \mu\text{g}/\text{m}^3$, 51%), Nanjing (27
37 $\mu\text{g}/\text{m}^3$, 55%), and Hefei ($24 \mu\text{g}/\text{m}^3$, 44%). Compared to the long-term policies from 2016 to 2019, the emergency emission
38 control measures implemented during the G20 Summit achieve more significant decreases in PM_{2.5} concentrations ($17 \mu\text{g}/\text{m}^3$
39 and 41%) over most of the whole domain, especially in Hangzhou ($24 \mu\text{g}/\text{m}^3$, 48%) and Shanghai ($21 \mu\text{g}/\text{m}^3$, 45%). By
40 extrapolation, we derive insight into the magnitude and spatial distribution of PM_{2.5} mitigation potential across the YRD,
41 revealing significantly additional room for curbing PM_{2.5} levels.

42 **1 INTRODUCTION**

43 Anthropogenic induced fine particulate matter (particulate matter with an aerodynamic diameter smaller than 2.5 μm ,
44 hereinafter denoted as PM_{2.5}) is a principal object of air pollution control in China (Huang et al., 2014; Zhang et al., 2015).
45 Moreover, the government has made major strides in curbing anthropogenic emissions (e.g., SO₂, NO_x, and CO) via both long-
46 term and emergency measures during the past decade (Yan et al., 2018; Yang et al., 2019; Zhang et al., 2012). However, owing
47 to the complex synergy of chemistry and meteorology (Seinfeld and Pandis, 2016), the extent to which these measures have
48 abated PM_{2.5} pollution, as well as the attainable mitigation potential, remains unclear (An et al., 2019).

49 *The main challenge involves reliably representing substantial and rapid changes in anthropogenic emissions resulting from*
50 *both long-term and emergency control measures (Chen et al., 2019; Cheng et al., 2019; Zhang et al., 2014; Yang et al., 2016;*
51 *Zhai et al., 2019; Zhang et al., 2019; Zhong et al., 2018). To gain timely insight into variations in anthropogenic emissions,*
52 *considerable efforts went into establishing detailed bottom-up emissions and derived valuable findings (Cheng et al., 2019;*
53 *Zhang et al., 2019). Yet bottom-up inventories were built on the basis of activity data as well as emission factors. These input*
54 *data can be absent or outdated, likely leading to misunderstandings of anthropogenic impacts, particularly in terms of the*

55 magnitude (Jiang et al., 2018). Recent studies applied available observations to construct multilinear regression models
56 (emission-based or meteorology-related), thus allowing us to separate contributions from anthropogenic emissions and
57 meteorology to some extent (Zhai et al., 2019; Zhong et al., 2018). However, the uncertainties in bottom-up inventories and
58 meteorology remained. Here we switched to observational constraints on a state-of-the-art chemical model. This can be a
59 potential way to tackle this challenge.

60 Since 2013, the China National Environmental Monitoring Center (CNEMC) has established 1415 ground-based PM_{2.5}
61 measurement sites across 367 key cities (Zhang and Cao, 2015). In contrast to satellite observations with sparse spatiotemporal
62 coverages (Ma et al., 2014, 2015; Xue et al., 2019), these ground sites can provide hourly PM_{2.5} concentrations at high spatial
63 resolution in urban areas. Data assimilation (DA) methods that have been widely used in meteorology can be extended to
64 integrate those continuous observational constraints with chemical transport models (CTMs) (Bocquet et al., 2015; Chai et al.,
65 2017; Gao et al., 2017; Jung et al., 2019; Ma et al., 2019). It has been demonstrated that the capability of several representative
66 DA methods, such as the optimal interpolation (OI) (Chai et al., 2017), 3D/4D variational methods (Li et al., 2016), and the
67 ensemble Kalman filter algorithm (Chen et al., 2019), can bridge the estimation gaps between observed and simulated results.
68 Thus, observational constraints can be taken full advantage of to identify the effects of anthropogenic emission controls.

69 From the perspective of policymaking, 2016 was a special year for air pollution control in China. Since 2013, the Chinese
70 government instituted extensive policies, such as the Air Pollution Prevention and Control Action Plan. These strategies were
71 initiated and implemented through generally shutting down or relocating high emission traditional industrial enterprises
72 (Sheehan et al., 2014; Shi et al., 2016; Xie et al., 2015). Starting from January 1, 2016, the relevant law, as well as the “Blue
73 Sky Battle Plan”, came into full effect and profoundly shifted how China prioritized air quality management (Feng and Liao,
74 2016; Li et al., 2019c). Hence, we address the impact of long-term emission control strategies on PM_{2.5} mitigation from 2016
75 onward.

76 The G20 summit hosted in Hangzhou in 2016 (hereinafter termed the G20 summit) provides a unique and ideal opportunity to
77 further explore the attainable PM_{2.5} mitigation potential across the Yangtze River Delta (YRD) (Li et al., 2017c; Ma et al.,
78 2019; Shu et al., 2019; Yang et al., 2019). Prior to and during this period, the Chinese government enforced historically strictest,
79 even unsustainable, emergency emission control measures, including significant control, even cessation, of factory operations,
80 restrictions on vehicles in the region, thus achieving significant PM_{2.5} abatement at specific locations (e.g., Hangzhou) (Ji et
81 al., 2018; Li et al., 2017c; Yang et al., 2019). Those measures were conducted across the whole YRD (including Zhejiang,
82 Jiangsu, and Anhui provinces, and Shanghai municipality), particularly in Hangzhou that served as the host city (Li et al.,
83 2019b, 2017c; Ni et al., 2020; Yu et al., 2018). Li et al. (2017) assumed that most of anthropogenic emissions (e.g., those from
84 industry, power plant, residential, and on-road transportation sectors) were reduced by around 50%. The role of these

85 emergency emission control measures, that is, the relatively localized PM_{2.5} mitigation potential, can thus be identified, and
86 further extended to the entire YRD.

87 To quantify the effectiveness of the emission control strategies, we constrained a state-of-the-art CTM by a reliable DA method
88 with extensive chemical and meteorological observations. This comprehensive technical design provides a crucial advance in
89 isolating the influences of emission changes and meteorological perturbations over the YRD from 2016 to 2019, thus deriving
90 estimates of PM_{2.5} responses to both long-term and emergency emission control measures, and establishing the first map of
91 the PM_{2.5} mitigation potential across the YRD.

92 **2 MATERIALS AND METHODS**

93 **2.1 The two-way coupled WRF-CMAQ model**

94 The two-way coupled Weather Research and Forecasting (WRF) and Community Multiscale Air Quality (CMAQ) model (the
95 WRF-CMAQ model), as the key core of the DA system, was applied to investigate the ambient PM_{2.5} feedbacks under different
96 constraining circumstances (Byun and Schere, 2006; Wong et al., 2012; Yu et al., 2013). We utilized the CB05 and AERO6
97 modules for gas-phase chemistry and aerosol evolution (Carlton et al., 2010; Yarwood et al., 2005), respectively. Both
98 secondary inorganic and organic aerosol (i.e., SIA and SOA) were thus explicitly treated with the AERO6 scheme in the WRF-
99 CMAQ model. Together with the ISORROPIA II thermodynamic equilibrium module (Fountoukis and Nenes, 2007), SIA in
100 the Aitken and accumulation modes (Binkowski and Roselle, 2003) was assumed to be in thermodynamic equilibrium with
101 the gas phase, while that in the coarse mode was treated dynamically. SOA was formed via gas-, aqueous-, and aerosol-phase
102 oxidation processes, such as in-cloud oxidation of glyoxal and methylglyoxal, absorptive partitioning of condensable oxidation
103 of monoterpenes, long alkanes, low-yield aromatic products (based on m-xylene data), and high-yield aromatics, and NO_x-
104 dependent yields from aromatic compounds (Carlton et al., 2010). The subsequent reaction products can be divided into two
105 groups: non-volatile semi-volatile. Such treatments have been widely used and comprehensively validated. Longwave and
106 shortwave radiation were both treated using the RRTMG radiation scheme (Clough et al., 2005). Related land surface energy
107 balance and planetary boundary layer simulations were included in the Pleim-Xiu land surface scheme (Xiu and Pleim, 2001)
108 and the asymmetric convective model (Pleim, 2007b, 2007a), respectively. The two-moment Morrison cloud microphysics
109 scheme (Morrison and Gettelman, 2008) and the Kain-Fritsch cumulus cloud scheme (Kain, 2004) were employed for
110 simulating aerosol-cloud interactions and precipitation. Default settings in the model were used to prescribe chemical initial
111 and boundary conditions. A spin-up period of seven days was carried out in advance to eliminate artefacts associated with
112 initial conditions. Meteorological initial and boundary conditions were obtained from the ECMWF reanalysis dataset with the
113 spatial resolution of 1° × 1° and temporal resolution of 6 hours (<http://www.ecmwf.int/products/data>, last access: 7 March

114 2020). Biogenic and dust emissions were calculated on-line using the Biogenic Emission Inventory System version 3.14
115 (BEISv3.14) (Carlton and Baker, 2011) and a windblown dust scheme embedded in CMAQ (Choi and Fernando, 2008),
116 respectively.

117 The horizontal domain of the model covered mainland China by a 395×345 grid with a 12 km horizontal resolution following
118 a Lambert Conformal Conic projection (Figure 1). In terms of the vertical configuration, 29 sigma-pressure layers ranged from
119 the surface to the upper level pressure of 100 hPa, 20 layers of which are located below around 3 km to derive finer
120 meteorological and chemical characteristics within the planetary boundary layer.

121 As a state-of-the-art CTM, the WRF-CMAQ model has been widely used to simulate spatiotemporal $PM_{2.5}$ distributions at
122 regional scales. However, model biases remain, mainly due to imperfect representations of chemical and meteorological
123 processes. Inaccurate anthropogenic emissions will exacerbate these biases. Therefore, external constraints on simulated results
124 enforced by the DA method will be taken into account in order to optimize spatiotemporal $PM_{2.5}$ distributions (Bocquet et al.,
125 2015).

126 **2.2 Anthropogenic emissions**

127 The anthropogenic emissions were obtained from the Multi-resolution Emission Inventory for China version 1.2 (MEIC)(Li
128 et al., 2017b), which contained primary species (e.g., primary $PM_{2.5}$, SO_2 , NO_x , CO, and NH_4) from five anthropogenic sectors
129 (i.e., agriculture, power plant, industry, residential, and transportation). This inventory was initially designed with the spatial
130 resolution of $0.25^\circ \times 0.25^\circ$ and thus needed to be reallocated to match the domain configuration (i.e., $12km \times 12km$) in the
131 study.

132 Recent findings show that MEIC generally provides reasonable estimates of total anthropogenic emissions for several typical
133 regions in China, such as the Beijing-Tianjin-Hebei region, the YRD, and the Pearl River Delta region (Li et al., 2017b).
134 Nevertheless, large uncertainties in spatial proxies (e.g., population density and road networks) still exist within these specific
135 regions (Geng et al., 2017). More, MEIC was originally constructed for the 2016 base year. Hence, owing to the impact of the
136 long-term emission control measures, MEIC was considered to be inappropriate for this study period (i.e., 2019).
137 Comparatively, emergency control measures could give rise to much more significant emission controls in the short term,
138 thereby leading to further uncertainties.

139 **2.3 Observational network**

140 To track real-time air quality in China, the National Environmental Monitoring Center (CNEMC, <http://www.cnemc.cn/>, last
141 access: 7 March 2020) has established 1415 sites across 367 cities since 2013 (Figure 1). Among these, 244 monitoring sites
142 were densely distributed in 6660 **grid cells** across the YRD providing hourly $PM_{2.5}$ measurements, resulting in **potentially**

143 excellent roles in constraining simulated PM_{2.5} (Bocquet et al., 2015). In this study, we applied observed PM_{2.5} concentrations
144 to constrain and evaluate the model performance. It is worth noting that the constraining capability of those observations varies
145 depending on specific configurations (e.g., the nature of the utilized DA method, the assimilation frequency, and the
146 representative errors of observations) (Bocquet et al., 2015; Chai et al., 2017; Ma et al., 2019; Rutherford, 1972). As shown in
147 Figure 1a, to consider regional impacts outside the YRD, the ground-level observations in the fan-shaped quadrilateral were
148 used to constrain the model performance. This was mainly due to the fact that this fan-shaped geographical scope covered
149 almost all key regions that had potentially regional impacts on the YRD, involving the Beijing-Tianjin-Hebei region (BTH),
150 the Pearl River Delta region, the Sichuan-Chongqing region, and the Shaanxi-Gansu region (Zhang et al., 2019). On the other
151 hand, the ground monitoring sites within the fan-shaped quadrilateral were significantly denser than those outside, thus leading
152 to much more effective DA results in practice (Bocquet et al., 2015; Chai et al., 2017). Collectively, to assimilate the
153 observations in the fan-shaped quadrilateral might be a sensible way to balance the DA effectiveness and the computing
154 efficiency. A resultant evidence lies in the model performance evaluation in Sect. 3.1, which would prove that this DA
155 configuration can enable reliable PM_{2.5} simulations.

156 2.4 Optimal interpolation

157 Optimal interpolation (OI) was chosen to assimilate hourly observations into the WRF-CMAQ model, aiming to generate the
158 accurate state of spatiotemporal PM_{2.5} distributions. Compared to the solely model-dependent results, this constraining method
159 relies on observations and thus makes it possible to minimize model uncertainties in optimizing the spatiotemporal PM_{2.5}
160 changes resulting from emission controls (Chai et al., 2017; Jung et al., 2019). The analysed states from the OI method were
161 calculated based on the following interpolation equation:

$$162 \quad \mathbf{X}^a = \mathbf{X}^b + \mathbf{B}\mathbf{H}^T(\mathbf{H}\mathbf{B}\mathbf{H}^T + \mathbf{O})^{-1}(\mathbf{Y} - \mathbf{H}\mathbf{X}^b) \quad (1)$$

163 where \mathbf{X}^a and \mathbf{X}^b denote the analysis (constrained) and background (simulated) values, respectively. \mathbf{B} and \mathbf{O} are background
164 and observation error-covariance matrices, respectively, for which we assumed no correlation in this study. \mathbf{H} refers to a
165 linearized observational operator, and \mathbf{Y} represents the observation vector. The OI method is described in detail in Adhikary
166 et al. (Adhikary et al., 2008).

167 Once available measurements were assimilated, the states of the simulated variables were adjusted from their background
168 values to corresponding analysis states using the scaling ratio $\mathbf{X}^a/\mathbf{X}^b$ obtained following equation (1). As the measurements
169 were conducted at the surface, this ratio at each grid cell was used to scale all aerosol components below the boundary layer
170 top. Such simplification compensated for the lack of information to constrain speciated aerosol components or their vertical
171 distributions. When ground-level PM_{2.5} measurements were assimilated, hourly observations were put into equation (1) to
172 construct the new analysis fields. All-day state variables associated with aerosols in the model were adjusted from their

173 background (simulated) to their analysis (constrained) states using the scaling factors ($\mathbf{X}^a/\mathbf{X}^b$). The adjusted model state
174 variables were then used to initiate the model to predict the next background state (\mathbf{X}^b) in Equation (1). Therefore, the
175 background state (\mathbf{X}^b) served as a prior model prediction before it was combined with the newly available observation (\mathbf{Y}) to
176 generate a new analysis state (\mathbf{X}^a) using Equation (1).

177 Measurements within the background-error correlation length scale were used to shape analysis states (\mathbf{X}^a). The background
178 error covariance \mathbf{COV}_{ij} between any two grid cells \mathbf{i} and \mathbf{j} was simulated as

$$179 \quad \mathbf{COV}_{ij} = \boldsymbol{\varepsilon}_i \boldsymbol{\varepsilon}_j e^{-\frac{\Delta_{ij}}{L}} \quad (2)$$

180 where $\boldsymbol{\varepsilon}_i$ and $\boldsymbol{\varepsilon}_j$ referred to the standard deviations of the background errors in two grid cells and Δ_{ij} denoted the distance
181 between the two grids. As a result, L was the background-error correlation length scale, which can be obtained by the
182 Hollingsworth-Lönnerberg method (Chai et al., 2017; Hollingsworth and Lönnerberg, 1986; Kumar et al., 2012). Figure 2 shows
183 the correlation coefficient, i.e., $\mathbf{COV}_{ij}/\boldsymbol{\varepsilon}_i \boldsymbol{\varepsilon}_j$, as a function of the separation distance between two grid cells, which was averaged
184 over 10 km bins. The results identified that a correlation length scale of ~ 180 km could be treated as the threshold. It allowed
185 the correlation coefficients to fall within the range of e^{-1} , defining the effective radius of each individual observation. Due to
186 the intensive monitoring sites in our study domain, this threshold was applied uniformly for the YRD. In this study,
187 observations beyond the background-error correlation length scale would have no effect on \mathbf{X}^a . Following Chai et al. (Chai et
188 al., 2017), the standard deviation of the background errors was assigned as 60% of the background values, while the
189 observational errors were assumed to be $\pm 20\%$ of the measurement values.

190 2.4 Experiment design

191 Anthropogenic emission controls and meteorological perturbations are both critical factors that dominate interannual and daily
192 variations in ambient $\text{PM}_{2.5}$ (Zhang et al., 2019). Our major objective is to isolate the impacts of emission-oriented long-term
193 and emergency measures and further explore the attainable $\text{PM}_{2.5}$ mitigation potential. We designed three sets of experiments,
194 which focused on three time periods, January 2016, January 2019, and the G20 period (from August 26, 2016 to September 7,
195 2016), respectively (Table 1).

196 For all experiments, the anthropogenic emissions were kept consistent (i.e., MEIC), while the ECMWF reanalysis datasets
197 accounted for the hourly observational constraints on spatiotemporal meteorological evolutions. The ECMWF reanalysis
198 datasets accounted for the hourly observational constraints on spatiotemporal meteorological evolutions. Therein almost all
199 necessary meteorological factors (nine variables), involving temperature, U wind component, V wind component, pressure,
200 relative humidity, precipitation, short-wave radiation, cloud cover, and planetary boundary layer height (PBLH), were
201 assimilated (<https://apps.ecmwf.int/datasets/data/interim-full-daily/levtype=sfc/>, last access: 7 March 2020). These

202 configurations unified both chemical (i.e., emission inventories) and meteorological input data for the WRF-CMAQ model.
203 Hence, the extent to which we introduce observational constraints on simulated $PM_{2.5}$ variations using the OI method is the
204 key to isolate the impacts of anthropogenic emission controls. Specifically, the differences in the constrained $PM_{2.5}$
205 concentrations between DA_2016 and DA_2019 reflected the net effects of anthropogenic emission controls and
206 meteorological perturbations between 2016 and 2019, while meteorological impacts therein were calculated as the
207 discrepancies in simulated $PM_{2.5}$ concentrations between NO_2016 and NO_2019 (Chen et al., 2019). Hence, by subtracting
208 meteorological impacts from the net effects, we can isolate the effects of anthropogenic emission controls attributable to the
209 long-term strategies.

210 The G20 summit provided a unique opportunity to realize the $PM_{2.5}$ mitigation potential in specific regions (Li et al., 2019a,
211 2017c; Ma et al., 2019; Shu et al., 2019; Yang et al., 2019). This is due to the fact that the Chinese government implemented
212 the most historically stringent, even unsustainable, strategies to curb anthropogenic emissions during that period in Hangzhou
213 and surrounding areas. To quantify the projected $PM_{2.5}$ abatement, we adopted the abovementioned method to constrain the
214 unique $PM_{2.5}$ variations in the DA_G20 experiment and further compared the corresponding results with those of the sole
215 model-dependent analysis (i.e., NO_G20). However, the subsequent discrepancies were related not only to the effects of
216 emergency anthropogenic emission strategies but also to the inherent biases mainly due to the emission inventory (Zhang et
217 al., 2019). In theory, such biases would generally remain unchanged in the short term when no emergency emission controls
218 occurred. Their consequent impacts could thus be stable under similar meteorological conditions. Therefore, to avoid additional
219 uncertainties, the adjacent periods of the G20 summit (i.e., pre- and post- periods, from August 11 to August 23, 2016 and
220 from September 18 to September 30, 2016, respectively) are the optimal alternative to eliminate the impacts of those inherent
221 biases. Figure S1 demonstrates the significantly similar meteorological fields among these three periods. As a result, the
222 corresponding experiments (i.e., DA_CON_G20 and NO_CON_G20) (Table 1) were conducted. By subtracting such
223 differences, we could isolate the $PM_{2.5}$ responses to the solely emergency anthropogenic emission strategies and finally achieve
224 the $PM_{2.5}$ mitigation potential for specific locations. Such localized $PM_{2.5}$ mitigation potential should be further expanded to
225 the entire YRD based on the impacts of both long-term and emergency strategies.

226 There is an essential prerequisite to above analysis. As the evaluation protocols, we need to verify that the DA experiments
227 (i.e., DA_2016, DA_2019, DA_G20, and DA_CON_G20) can reproduce the spatiotemporal variations in the $PM_{2.5}$ and major
228 meteorological fields (i.e., temperature, relative humidity, wind speed and air pressure) (Chai et al., 2017). While 244
229 monitoring stations reside in 6660 grid cells, 16 grid cells have two to three monitors in them. For these grid cells, only one
230 averaged measurement was used for DA. However, all the observations were compared against the constrained results.
231 Although SIA and SOA are key components of the ambient $PM_{2.5}$, extensive measurements at the regional scale of these
232 components are generally lacking. It is thus difficult to generate appropriate constraints on SIA and SOA (Chai et al., 2017;

233 Gao et al., 2017). Note that different anthropogenic emissions might lead to inconsistent estimation of meteorological effects
234 on ambient PM_{2.5} (Chen et al., 2019). To eliminate this doubt, we conducted sensitivity tests by reducing MEIC with three
235 reasonable ratios (i.e., -5%, -25%, and -40%) over the YRD based on NO₂₀₁₆ and NO₂₀₁₉.

236 3 RESULTS

237 3.1 Data assimilation performance

238 Figure 3 shows spatial comparisons of hourly averaged concentrations of constrained and simulated PM_{2.5} (i.e., the ones from
239 the cases with and without DA, respectively) with ground-level observations across the YRD for January 2016, January 2019,
240 and the G20 summit. In the NO₂₀₁₆, NO₂₀₁₉, and NO_{G20} experiments, the simulated PM_{2.5} concentrations generally
241 overestimated observed values by 16 ~ 57 µg/m³, especially those in Hangzhou and surrounding areas during the G20 summit
242 (> 21 µg/m³). Such prevailing overestimates were mainly a result of the anthropogenic emission inventory (i.e., MEIC), as a
243 bottom-up product, which notably cannot capture interannual emission changes since the base year 2012, as well as the large
244 emission controls resulting from the emergency controls during the G20 summit. By comparison, the constrained results
245 significantly approach observations. Specifically, in the DA₂₀₁₆, DA₂₀₁₉, and DA_{G20} cases, the biases of the assimilated
246 PM_{2.5} were all constrained in an extremely narrow range (i.e., 10 µg/m³, 12 µg/m³, and 13 µg/m³, respectively), suggesting that
247 the DA method can reproduce the spatiotemporal distributions of surface PM_{2.5} at the regional scale.

248 To achieve more targeted evaluations, it is necessary to further assess the ability of the DA method in reproducing the city-
249 level PM_{2.5} responses. With the analysis of time series over the same periods, Figure 4 illustrates the comparisons between
250 hourly observed, simulated, and constrained PM_{2.5} concentrations over the whole domain and four representative cities (i.e.,
251 Shanghai, Hangzhou, Nanjing, and Hefei). Similar to the spatial comparisons, the constrained PM_{2.5} generally reproduces the
252 temporal variations in observations, while the model-dependent simulated results are prone to overestimating those
253 observations, in particular, the peaks by 85 ~ 257 µg/m³.

254 As expected, basic evaluation indicators (i.e., the NMB and R values) of assimilated PM_{2.5} exhibited significantly better
255 behaviour than those without constraints (Figure S2). Taking the simulated and assimilated results for Hangzhou during
256 January 2016 as an example, the corresponding R values improved from 0.63 to 0.98, while the NMB values were reduced
257 from 17% to 3%. Similar improvements, but with varying extent, were found in other paired experiments.

258 Owing to the fact that the distinct PM_{2.5} levels might also play a potential role in the DA performance, we thus separated the
259 entire range of the observed PM_{2.5} concentrations into four intervals (i.e., < 35 µg/m³, 35 ~ 75 µg/m³, 75 ~ 115 µg/m³, and >
260 115 µg/m³), exactly corresponding to the continuously increasing PM_{2.5} levels. Figure S3 demonstrates that, relative to the sole
261 model-dependent configurations, this constraining method could substantially strengthen the model performance, especially

262 for the relatively elevated concentration intervals. Overall, the ranges of the NMB values and associated standard deviations
263 decreased from -24 ~ 86% to -9 ~ 25% and 34 ~ 174 $\mu\text{g}/\text{m}^3$ to 12 ~ 52 $\mu\text{g}/\text{m}^3$, respectively. Theoretically, more frequent DA
264 should lead to more robust simulations. Hourly observational constraints on the $\text{PM}_{2.5}$ concentrations were thus adopted to
265 tackle this issue. This is the reason why the corresponding NMB values in the constraining cases roughly maintain stability,
266 fluctuating over a narrow range (i.e., $\pm 20\%$) in the study periods (Figure S4). In addition, given the fact that the assimilated
267 ERA reanalysis dataset has much wider spatial coverage than ground-based measurements, we also reproduced the
268 spatiotemporal variations in the meteorological factors (e.g., temperature, relative humidity, wind speed, and air pressure)
269 (Figures S5 ~ S8). Together the comprehensive evaluation statistics as summarized in Tables S1 ~ S5, it has been demonstrated
270 that the DA method can enable one to derive not only reliable $\text{PM}_{2.5}$ evolution but also accurate meteorological fields. Regional
271 transport of $\text{PM}_{2.5}$ can thus be captured reasonably in this way.

272 3.2 Ambient $\text{PM}_{2.5}$ responses to the long-term strategies

273 The Chinese government has been implementing stringent emission control strategies since 2016, especially in the YRD (Feng
274 and Liao, 2016; Li et al., 2019c). To quantify subsequent $\text{PM}_{2.5}$ responses is thus the prerequisite to our final objective, that is,
275 to explore the associated $\text{PM}_{2.5}$ mitigation potential.

276 Interannual changes in spatiotemporal $\text{PM}_{2.5}$ distributions depended strongly on both anthropogenic emission controls and
277 meteorological variations from 2016 to 2019. Their combined effects were reflected by the differences between the constrained
278 results from DA_2016 and DA_2019. As shown in Figure 5a, such net impacts led to prevailing $\text{PM}_{2.5}$ abatement in the domain,
279 especially in megacities, such as Shanghai (13 $\mu\text{g}/\text{m}^3$, 21%), Hangzhou (13 $\mu\text{g}/\text{m}^3$, 17%), Nanjing (6 $\mu\text{g}/\text{m}^3$, 8%), and Hefei (2
280 $\mu\text{g}/\text{m}^3$, 2%). In addition, noticeable $\text{PM}_{2.5}$ controls also occurred in the western and northern YRD, where abundant
281 anthropogenic emissions are concentrated (Figure S9). Detailed differences are shown in Table S6.

282 Figure 5b highlights that the sole meteorological interferences played an extensively positive role in increasing the regional
283 $\text{PM}_{2.5}$ concentrations for most areas of the domain ($\sim 12 \mu\text{g}/\text{m}^3$, 15%). This also indirectly implied the importance of
284 assimilating meteorology, which, however, were generally neglected by previous studies (Chen et al., 2019). In this study, we
285 have eliminated this speculation. As shown in Figure S10 and Figure 5, even with the largest adjustment (i.e., -40%), such
286 interferences could be well controlled within the 5% ($< 3 \mu\text{g}/\text{m}^3$) scope, let alone other tests (i.e., $< 3\%$, $< 2 \mu\text{g}/\text{m}^3$). Moreover,
287 these findings are consistent with previous analyses (Chen et al., 2019; Zhang et al., 2019). They generally reveal that
288 reasonable changes in the bottom-up emissions, together with the same meteorology input data, would not remarkably alter
289 the simulated results associated with meteorological effects on surface $\text{PM}_{2.5}$ ($< 5\%$). As a result, some past studies even
290 directly ignored such sensitivity tests without any discussion (Chen et al., 2019). Therefore, by subtracting those
291 meteorological influences from the combined outcomes, we can finally derive the contributions of anthropogenic emission

292 controls to the PM_{2.5} mitigation at the regional scale. Figure 5c illustrates that long-term emission control strategies from 2016
293 to 2019 produced substantial (> 14 µg/m³, 19%) decreases in regional PM_{2.5} concentrations, which are similar to those
294 combined effects in terms of the spatial distributions.

295 For the entire domain, as well as the four representative cities, the synergy between anthropogenic emission controls and
296 meteorological interferences on the PM_{2.5} concentrations were calculated at the city level (Figure 6). We found that their net
297 effects resulted in uniformly positive mitigations as follows: -2 µg/m³ (-3%), -13 µg/m³ (-21%), -12 µg/m³ (-17%), -6 µg/m³
298 (-8%), and -2 µg/m³ (-3%) for the whole domain, Shanghai, Hangzhou, Nanjing, and Hefei, respectively, while the
299 meteorological conditions therein offset such effects to different extents (5 ~ 18 µg/m³, 16 ~ 24%). We recognized that the
300 impacts of anthropogenic drivers on PM_{2.5} concentrations in the southern and eastern parts of Zhejiang were evidently weaker
301 than those in other regions in the YRD. This divergence can mostly be explained by spatial distributions of anthropogenic
302 emissions. That is, anthropogenic emissions in the southern and eastern of Zhejiang were also significantly less than those in
303 other regions (Figure S9), thus leading to substantially low PM_{2.5} concentrations (Figure 3). Besides, meteorological fields in
304 coastal regions, more conducive to PM_{2.5} diffusion (Figure 5), might be another cause. The above findings confirmed that the
305 PM_{2.5} mitigation was dominated by anthropogenic emission controls, rather than meteorological variations. Furthermore, the
306 corresponding spatiotemporal patterns were highly correlated to those of the anthropogenic emissions (Figure S9). This
307 indicates that the impacts of the long-term strategies are mainly driven by anthropogenic emission mitigation.

308 3.3 Ambient PM_{2.5} mitigation potential

309 The G20 summit offered a unique and ideal opportunity to clarify the effects of the most stringent emission control measures
310 across the YRD from 2016 to 2019, which could be regarded as the localized PM_{2.5} mitigation potential. Figure 7a shows the
311 spatial differences between the constrained and simulated PM_{2.5} concentrations, which were extracted from DA_G20 and
312 NO_G20, for the period of the G20 summit. Inherent biases remained, primarily attributable to the priori anthropogenic
313 emissions. Their subsequent impacts were then quantified by comparing the discrepancies between the results from two
314 additional experiments (i.e., DA_CON_G20 and NO_CON_G20) (Figure 7b). More, such impacts were associated with
315 relatively low standard deviations (< 5%), thus presenting a stably spatiotemporal state (Figure S11). This means that such
316 estimations were also suitable for the G20 summit. Therefore, by subtracting them, the re-corrected differences would reflect
317 the actual effects of the most stringent emission control measures for the G20 summit (Figure 7c). Such hotspots with extremely
318 negative values reveal the dramatic PM_{2.5} mitigations for these specific locations. The corresponding largest decreases in PM_{2.5}
319 concentrations (35 µg/m³, 59%) occurred in Hangzhou and its surrounding areas, as expected. Following Hangzhou, other
320 hotspots with relatively prominent declines also emerged in megacities, especially in Shanghai (32 µg/m³, 51%), Nanjing (27
321 µg/m³, 55%) and Hefei (24 µg/m³, 44%). This behaviour could be explained by two inferences that: (i) local emission controls

322 in Hangzhou were projected to be conducted with the maximum execution efficiency compared to those in surrounding regions;
323 (ii) most of the emergency measurements generally targeted the vehicle and industry emissions that are clustered around the
324 urban rather than rural areas.

325 Compared to the long-term policies from 2016 to 2019, the emergency emission control measures implemented during the
326 G20 Summit achieved more significant decreases in $\text{PM}_{2.5}$ concentrations ($17 \mu\text{g}/\text{m}^3$ and 41%) over most of the whole domain,
327 especially in Hangzhou ($24 \mu\text{g}/\text{m}^3$, 48%) and Shanghai ($21 \mu\text{g}/\text{m}^3$, 45%) (Figure 8). Detailed differences are summarized in
328 Table S6.

329 To gain the regional $\text{PM}_{2.5}$ mitigation potential, (i) we first pinpointed the main urban areas of Hangzhou that covered 25 grid
330 cells (Figure S12), in which the most substantial $\text{PM}_{2.5}$ abatement, i.e., the localized $\text{PM}_{2.5}$ mitigation potential ($> 22 \mu\text{g}/\text{m}^3$
331 and $> 59\%$) were identified. (ii) As the above hypothesis, the spatial distributions of the regional $\text{PM}_{2.5}$ mitigation potential
332 across the YRD were then assumed to follow those of the long-term strategy effects. (iii) Thus, by extrapolation in equal
333 proportion following such patterns and the localized $\text{PM}_{2.5}$ mitigation potential, we established the map of the $\text{PM}_{2.5}$ mitigation
334 potential across the YRD (Figure 9a). It should be noted that, as long as three premises, including typical weather backgrounds,
335 [stable structures of anthropogenic emissions](#), and analogous emission control measures, remain unchanged, Figure 9a is a
336 reliably quantitative reference to characterize the attainable $\text{PM}_{2.5}$ abatement for the YRD in future.

337 **4 DISCUSSION**

338 The actual effectiveness of anthropogenic emission control measures, especially those directed at $\text{PM}_{2.5}$ mitigation, has long
339 been excluded from evaluation of air pollution policies in China, in part due to the complex synergy between anthropogenic
340 emissions and meteorology. Here, we provide a novel approach to explore the $\text{PM}_{2.5}$ responses to anthropogenic emission
341 control measures and their mitigation potential from 2016 to 2019 across the YRD, China. With the data assimilation method,
342 these estimates are projected to be highly reliable due to the sufficient observational constraints. The results demonstrate that
343 long-term anthropogenic emission control strategies from 2016 to 2019 have led to extensive impacts on $\text{PM}_{2.5}$ abatement
344 across the YRD, especially in the megacities, Shanghai, Hangzhou, Nanjing, and Hefei. In the context of the G20 summit, the
345 emergency strategies could achieve significant $\text{PM}_{2.5}$ abatement ($> 50\%$) at specific locations, (i.e., urban Hangzhou),
346 representing the localized mitigation potential. By extrapolation based on the above results, we have established the first map
347 of the $\text{PM}_{2.5}$ mitigation potential for the YRD.

348 Numerous analyses have focused on Hangzhou during the G20 summit to detect impacts of emergency emission controls (Li
349 et al., 2019b, 2017c; Yu et al., 2018). However, previous analyses generally found more effective predictions ($> 50\%$) at the
350 city level. This discrepancy might be related to the fact that such results were generally based on sole model-dependent
351 predictions, which are normally driven by uncertain bottom-up estimates of anthropogenic emissions. In addition, this study

352 addresses the YRD after 2016. Besides, similar opportunities also occurred at other spatiotemporal scales, such as the “APEC
353 Blue” in 2014 and “Parade Blue” in 2015 over the BTH (Liu et al., 2016; Sun et al., 2016; Zhang et al., 2016). More aggressive
354 achievements (> 55%) were generally attributed to emergency anthropogenic emission control measures (Sun et al., 2016).
355 This might be related to the fact that, compared to the YRD, the BTH is associated with more abundant primary emissions
356 (Zhang et al., 2019). The impacts of natural sources (e.g., biogenic emissions, wild fires, and natural dust) are not considered
357 in this study. This is mainly because of two reasons. First, it has been widely demonstrated that biogenic emission changes are
358 dominated by meteorological variations over a period of a few years (Wang et al., 2019). [Moreover, the former is generally of
359 minor significance for interannual PM_{2.5} variations for the YRD](#) (Mu and Liao, 2014; Tai et al., 2012). Second, satellite
360 products, including MOD14 and AIRIBQAP_NRT.005 (<https://worldview.earthdata.nasa.gov/>), show that there was no
361 noticeable wild fires and natural dust storms during this study period, thus allowing us to ignore the corresponding interferes.
362 This study takes the advantage of observational constraints to gain the regional PM_{2.5} mitigation potential. It could be further
363 optimized by more extensive observations. Besides, extending the PM_{2.5} mitigation potential in urban Hangzhou during the
364 study period to the entire YRD in other time periods may introduce some uncertainties due to varying meteorology. As
365 abovementioned, impacts of the extreme emergency emission controls are spatially inconsistent across the YRD. To explore
366 regional PM_{2.5} mitigation potential, it is thus unavoidable to extrapolate from local to regional scale. The consequent
367 uncertainty mainly relates to the hypothesis that the spatial patterns of the PM_{2.5} mitigation potential across the YRD should
368 follow those of the impacts of the long-term emission control strategies. In addition, there are distinct DA methods (Bocquet
369 et al., 2015). It is thus believed that replacing the OI with another DA algorithm would lead to slightly different results. [Note
370 that, as previous studies have demonstrated \(Cheng et al., 2019; Zhai et al., 2019; Zhong et al., 2018\), model uncertainties
371 remain, although we have verified the constrained results. We have supplemented the additional discussions in Sect. 4 for
372 further explanation. For instance, model simulations of aerosol components \(e.g., sulfate and nitrate\) are still poorly
373 constrained. Moreover, they have not been evaluated due to lack of available observations. Yet previous studies find that the
374 model tends to underestimate sulfate production during high RH and SOA \(Li et al., 2017a; Wang et al., 2014; Zhong et al.,
375 2018\). As a result, these uncertainties can be propagated into the estimations of meteorological effects. Besides, like other
376 atmospheric chemical transport models, the WRF-CMAQ model cannot provide model uncertainty information, while Monte
377 Carlo simulations for complex CTMs would be unrealistic due to extremely high computation loadings \(Zhong et al., 2018\).](#)
378 Looking forward, continued advances in observational techniques, better understanding of chemical and meteorological
379 processes, and their improved representations in CTMs are all factors that are critical to optimizing the estimates of the PM_{2.5}
380 mitigation potential.

381 **ASSOCIATED CONTENT**

382 **Supporting Information.**

383 The supplement related to this article is available online.

384 **NOTES**

385 The authors declare no competing financial interest.

386 **ACKNOWLEDGEMENTS**

387 This study was supported by the Department of Science and Technology of China (No. 2016YFC0202702, 2018YFC0213506
388 and 2018YFC0213503), National Research Program for Key Issues in Air Pollution Control in China (No. DQGG0107) and
389 National Natural Science Foundation of China (No. 21577126 and 41561144004). Pengfei Li is supported by Initiation Fund
390 for Introducing Talents of Hebei Agricultural University (412201904) and Hebei Youth Top Fund (BJ2020032).

391 **REFERENCES**

- 392 Adhikary, B., Kulkarni, S., Dallura, A., Tang, Y., Chai, T., Leung, L. R., Qian, Y., Chung, C. E., Ramanathan, V. and
393 Carmichael, G. R.: A regional scale chemical transport modeling of Asian aerosols with data assimilation of AOD
394 observations using optimal interpolation technique, *Atmos. Environ.*, 42(37), 8600–8615, 2008.
- 395 An, Z., Huang, R.-J., Zhang, R., Tie, X., Li, G., Cao, J., Zhou, W., Shi, Z., Han, Y., Gu, Z. and others: Severe haze in
396 Northern China: A synergy of anthropogenic emissions and atmospheric processes, *Proc. Natl. Acad. Sci.*, 116(18), 8657–
397 8666, 2019.
- 398 Binkowski, F. S. and Roselle, S. J.: Models-3 Community Multiscale Air Quality (CMAQ) model aerosol component 1.
399 Model description, *J. Geophys. Res. Atmos.*, 108(D6), 2003.
- 400 Bocquet, M., Elbern, H., Eskes, H., Hirtl, M., Žabkar, R., Carmichael, G. R., Flemming, J., Inness, A., Pagowski, M., Pérez
401 Camañó, J. L. and others: Data assimilation in atmospheric chemistry models: current status and future prospects for coupled
402 chemistry meteorology models, *Atmos. Chem. Phys.*, 15(10), 5325–5358, 2015.
- 403 Byun, D. and Schere, K. L.: Review of the governing equations, computational algorithms, and other components of the
404 Models-3 Community Multiscale Air Quality (CMAQ) modeling system, *Appl. Mech. Rev.*, 59(2), 51–77, 2006.
- 405 Carlton, A. G. and Baker, K. R.: Photochemical modeling of the Ozark isoprene volcano: MEGAN, BEIS, and their impacts
406 on air quality predictions, *Environ. Sci. Technol.*, 45(10), 4438–4445, 2011.

407 Carlton, A. G., Bhawe, P. V., Napelenok, S. L., Edney, E. O., Sarwar, G., Pinder, R. W., Pouliot, G. A. and Houyoux, M.:
408 Model representation of secondary organic aerosol in CMAQv4. 7, *Environ. Sci. Technol.*, 44(22), 8553–8560, 2010.

409 Chai, T., Kim, H.-C., Pan, L., Lee, P. and Tong, D.: Impact of Moderate Resolution Imaging Spectroradiometer Aerosol
410 Optical Depth and AirNow PM_{2.5} assimilation on Community Multi-scale Air Quality aerosol predictions over the
411 contiguous United States, *J. Geophys. Res. Atmos.*, 122(10), 5399–5415, 2017.

412 Chen, D., Liu, Z., Ban, J., Zhao, P. and Chen, M.: Retrospective analysis of 2015--2017 wintertime PM_{2.5} in China:
413 response to emission regulations and the role of meteorology, *Atmos. Chem. Phys.*, 19(11), 7409–7427, 2019.

414 Cheng, J., Su, J., Cui, T., Li, X., Dong, X., Sun, F., Yang, Y., Tong, D., Zheng, Y., Li, Y. and others: Dominant role of
415 emission reduction in PM_{2.5} air quality improvement in Beijing during 2013--2017: A model-based decomposition analysis,
416 *Atmos. Chem. Phys.*, 19(9), 6125–6146, 2019.

417 Choi, Y.-J. and Fernando, H. J. S.: Implementation of a windblown dust parameterization into MODELS-3/CMAQ:
418 Application to episodic PM events in the US/Mexico border, *Atmos. Environ.*, 42(24), 6039–6046, 2008.

419 Clough, S. A., Shephard, M. W., Mlawer, E. J., Delamere, J. S., Iacono, M. J., Cady-Pereira, K., Boukabara, S. and Brown,
420 P. D.: Atmospheric radiative transfer modeling: a summary of the AER codes, *J. Quant. Spectrosc. Radiat. Transf.*, 91(2),
421 233–244, 2005.

422 Feng, L. and Liao, W.: Legislation, plans, and policies for prevention and control of air pollution in China: achievements,
423 challenges, and improvements, *J. Clean. Prod.*, 112, 1549–1558, 2016.

424 Fountoukis, C. and Nenes, A.: ISORROPIA II: a computationally efficient thermodynamic equilibrium model for K⁺--Ca
425 ²⁺--Mg ²⁺--NH ⁴⁺--Na⁺--SO ₄ ²⁻--NO ₃⁻--Cl⁻--H ₂ O aerosols, *Atmos. Chem. Phys.*, 7(17), 4639–4659, 2007.

426 Gao, M., Saide, P. E., Xin, J., Wang, Y., Liu, Z., Wang, Y., Wang, Z., Pagowski, M., Guttikunda, S. K. and Carmichael, G.
427 R.: Estimates of health impacts and radiative forcing in winter haze in eastern China through constraints of surface PM_{2.5}
428 predictions, *Environ. Sci. Technol.*, 51(4), 2178–2185, 2017.

429 Geng, G., Zhang, Q., Martin, R. V., Lin, J., Huo, H., Zheng, B., Wang, S. and He, K.: Impact of spatial proxies on the
430 representation of bottom-up emission inventories: A satellite-based analysis., *Atmos. Chem. Phys.*, 17(6), 2017.

431 Hollingsworth, A. and Lönnerberg, P.: The statistical structure of short-range forecast errors as determined from radiosonde
432 data. Part I: The wind field, *Tellus A*, 38(2), 111–136, 1986.

433 Huang, R.-J., Zhang, Y., Bozzetti, C., Ho, K.-F., Cao, J.-J., Han, Y., Daellenbach, K. R., Slowik, J. G., Platt, S. M.,
434 Canonaco, F. and others: High secondary aerosol contribution to particulate pollution during haze events in China, *Nature*,
435 514(7521), 218, 2014.

436 Ji, Y., Qin, X., Wang, B., Xu, J., Shen, J., Chen, J., Huang, K., Deng, C., Yan, R., Xu, K. and others: Counteractive effects
437 of regional transport and emission control on the formation of fine particles: a case study during the Hangzhou G20 summit,
438 *Atmos. Chem. Phys.*, 18(18), 13581–13600, 2018.

439 Jiang, Z., McDonald, B. C., Worden, H., Worden, J. R., Miyazaki, K., Qu, Z., Henze, D. K., Jones, D. B. A., Arellano, A. F.,
440 Fischer, E. V and others: Unexpected slowdown of US pollutant emission reduction in the past decade, *Proc. Natl. Acad.*
441 *Sci.*, 115(20), 5099–5104, 2018.

442 Jung, J., Souri, A. H., Wong, D. C., Lee, S., Jeon, W., Kim, J. and Choi, Y.: The Impact of the Direct Effect of Aerosols on
443 Meteorology and Air Quality Using Aerosol Optical Depth Assimilation During the KORUS-AQ Campaign, *J. Geophys.*
444 *Res. Atmos.*, 124(14), 8303–8319, 2019.

445 Kain, J. S.: The Kain-Fritsch convective parameterization: an update, *J. Appl. Meteorol.*, 43(1), 170–181, 2004.

446 Kumar, U., De Ridder, K., Lefebvre, W. and Janssen, S.: Data assimilation of surface air pollutants (O₃ and NO₂) in the
447 regional-scale air quality model AURORA, *Atmos. Environ.*, 60, 99–108,
448 doi:<https://doi.org/10.1016/j.atmosenv.2012.06.005>, 2012.

449 Li, B., Wang, F., Yin, H. and Li, X.: Mega events and urban air quality improvement: A temporary show?, *J. Clean. Prod.*,
450 217, 116–126, 2019a.

451 Li, G., Bei, N., Cao, J., Huang, R., Wu, J., Feng, T., Wang, Y., Liu, S., Zhang, Q., Tie, X. and Molina, L. T.: A possible
452 pathway for rapid growth of sulfate during haze days in China, *Atmos. Chem. Phys.*, 17(5), 3301–3316, doi:10.5194/acp-17-
453 3301-2017, 2017a.

454 Li, H., Wang, D., Cui, L., Gao, Y., Huo, J., Wang, X., Zhang, Z., Tan, Y., Huang, Y., Cao, J. and others: Characteristics of
455 atmospheric PM_{2.5} composition during the implementation of stringent pollution control measures in Shanghai for the 2016
456 G20 summit, *Sci. Total Environ.*, 648, 1121–1129, 2019b.

457 Li, K., Jacob, D. J., Liao, H., Zhu, J., Shah, V., Shen, L., Bates, K. H., Zhang, Q. and Zhai, S.: A two-pollutant strategy for
458 improving ozone and particulate air quality in China, *Nat. Geosci.*, 12(11), 906–910, 2019c.

459 Li, M., Zhang, Q., Kurokawa, J., Woo, J.-H., He, K., Lu, Z., Ohara, T., Song, Y., Streets, D. G., Carmichael, G. R. and
460 others: MIX: a mosaic Asian anthropogenic emission inventory under the international collaboration framework of the
461 MICS-Asia and HTAP, *Atmos. Chem. Phys.*, 17(2), 2017b.

462 Li, P., Wang, L., Guo, P., Yu, S., Mehmood, K., Wang, S., Liu, W., Seinfeld, J. H., Zhang, Y., Wong, D. C. and others: High
463 reduction of ozone and particulate matter during the 2016 G-20 summit in Hangzhou by forced emission controls of industry
464 and traffic, *Environ. Chem. Lett.*, 15(4), 709–715, 2017c.

465 Li, X., Choi, Y., Czader, B., Roy, A., Kim, H., Lefer, B. and Pan, S.: The impact of observation nudging on simulated
466 meteorology and ozone concentrations during DISCOVER-AQ 2013 Texas campaign, *Atmos. Chem. Phys.*, 16(5), 3127–
467 3144, 2016.

468 Liu, H., Liu, C., Xie, Z., Li, Y., Huang, X., Wang, S., Xu, J. and Xie, P.: A paradox for air pollution controlling in China
469 revealed by “APEC Blue” and “Parade Blue,” *Sci. Rep.*, 6(1), 1–13, 2016.

470 Ma, C., Wang, T., Mizzi, A. P., Anderson, J. L., Zhuang, B., Xie, M. and Wu, R.: Multi-constituent data assimilation with
471 WRF-Chem/DART: Potential for adjusting anthropogenic emissions and improving air quality forecasts over eastern China,
472 *J. Geophys. Res. Atmos.*, 2019.

473 Ma, Z., Hu, X., Huang, L., Bi, J. and Liu, Y.: Estimating ground-level PM_{2.5} in China using satellite remote sensing,
474 *Environ. Sci. Technol.*, 48(13), 7436–7444, 2014.

475 Ma, Z., Hu, X., Sayer, A. M., Levy, R., Zhang, Q., Xue, Y., Tong, S., Bi, J., Huang, L. and Liu, Y.: Satellite-based
476 spatiotemporal trends in PM_{2.5} concentrations: China, 2004–2013, *Environ. Health Perspect.*, 124(2), 184–192, 2015.

477 Morrison, H. and Gettelman, A.: A new two-moment bulk stratiform cloud microphysics scheme in the Community
478 Atmosphere Model, version 3 (CAM3). Part I: Description and numerical tests, *J. Clim.*, 21(15), 3642–3659, 2008.

479 Mu, Q. and Liao, H.: Simulation of the interannual variations of aerosols in China: role of variations in meteorological
480 parameters, *Atmos. Chem. Phys.*, 14, 11177–11219, 2014.

481 Ni, Z.-Z., Luo, K., Gao, Y., Gao, X., Jiang, F., Huang, C., Fan, J.-R., Fu, J. S. and Chen, C.-H.: Spatial--temporal variations
482 and process analysis of O_3 pollution in Hangzhou during the G20 summit, *Atmos. Chem. Phys.*, 20(10), 5963–
483 5976, doi:10.5194/acp-20-5963-2020, 2020.

484 Pleim, J. E.: A combined local and nonlocal closure model for the atmospheric boundary layer. Part I: Model description and
485 testing, *J. Appl. Meteorol. Climatol.*, 46(9), 1383–1395, 2007a.

486 Pleim, J. E.: A combined local and nonlocal closure model for the atmospheric boundary layer. Part II: Application and
487 evaluation in a mesoscale meteorological model, *J. Appl. Meteorol. Climatol.*, 46(9), 1396–1409, 2007b.

488 RenHe, Z., Li, Q. and Zhang, R.: Meteorological conditions for the persistent severe fog and haze event over eastern China
489 in January 2013, *Sci. China Earth Sci.*, 57(1), 26–35, doi:10.1007/s11430-013-4774-3, 2014.

490 Rutherford, I. D.: Data assimilation by statistical interpolation of forecast error fields, *J. Atmos. Sci.*, 29(5), 809–815, 1972.

491 Seinfeld, J. H. and Pandis, S. N.: *Atmospheric chemistry and physics: from air pollution to climate change*, John Wiley &
492 Sons., 2016.

493 Sheehan, P., Cheng, E., English, A. and Sun, F.: China’s response to the air pollution shock, *Nat. Clim. Chang.*, 4(5), 306,
494 2014.

495 Shi, H., Wang, Y., Chen, J. and Huisingh, D.: Preventing smog crises in China and globally, *J. Clean. Prod.*, 112, 1261–
496 1271, 2016.

497 Shu, L., Wang, T., Han, H., Xie, M., Chen, P., Li, M. and Wu, H.: Summertime ozone pollution in the Yangtze River Delta
498 of eastern China during 2013--2017: Synoptic impacts and source apportionment, *Environ. Pollut.*, 113631, 2019.

499 Sun, Y., Wang, Z., Wild, O., Xu, W., Chen, C., Fu, P., Du, W., Zhou, L., Zhang, Q., Han, T. and others: “APEC blue”:
500 secondary aerosol reductions from emission controls in Beijing, *Sci. Rep.*, 6, 20668, 2016.

501 Tai, A. P. K., Mickley, L. J. and Jacob, D. J.: Impact of 2000--2050 climate change on fine particulate matter (PM_{2.5}) air
502 quality inferred from a multi-model analysis of meteorological modes, *Atmos. Chem. Phys.*, 2012.

503 Wang, P., Guo, H., Hu, J., Kota, S. H., Ying, Q. and Zhang, H.: Responses of PM_{2.5} and O₃ concentrations to changes of
504 meteorology and emissions in China, *Sci. Total Environ.*, 662, 297–306, 2019.

505 Wang, Y., Zhang, Q., Jiang, J., Zhou, W., Wang, B., He, K., Duan, F., Zhang, Q., Philip, S. and Xie, Y.: Enhanced sulfate
506 formation during China’s severe winter haze episode in January 2013 missing from current models, *J. Geophys. Res.*
507 *Atmos.*, 119(17), 10,410-425,440, doi:10.1002/2013JD021426, 2014.

508 Wong, D. C., Pleim, J., Mathur, R., Binkowski, F., Otte, T., Gilliam, R., Pouliot, G., Xiu, A., Young, J. O. and Kang, D.:
509 WRF-CMAQ two-way coupled system with aerosol feedback: software development and preliminary results, *Geosci. Model*
510 *Dev.*, 5(2), 299–312, 2012.

511 Xie, H., Wang, L., Ling, X., Miao, Y., Shen, X., Wang, M. and Xin, Y.: China air quality management assessment report
512 (2016), 2015.

513 Xiu, A. and Pleim, J. E.: Development of a land surface model. Part I: Application in a mesoscale meteorological model, *J.*
514 *Appl. Meteorol.*, 40(2), 192–209, 2001.

515 Xue, T., Zheng, Y., Tong, D., Zheng, B., Li, X., Zhu, T. and Zhang, Q.: Spatiotemporal continuous estimates of PM_{2.5}
516 concentrations in China, 2000--2016: A machine learning method with inputs from satellites, chemical transport model, and
517 ground observations, *Environ. Int.*, 123, 345–357, 2019.

518 Yan, B., Liu, S., Zhao, B., Li, X., Fu, Q. and Jiang, G.: China’s fight for clean air and human health, 2018.

519 Yang, W., Yuan, G. and Han, J.: Is China’s air pollution control policy effective? Evidence from Yangtze River Delta cities,
520 *J. Clean. Prod.*, 220, 110–133, 2019.

521 Yang, Y., Liao, H. and Lou, S.: Increase in winter haze over eastern China in recent decades: Roles of variations in
522 meteorological parameters and anthropogenic emissions, *J. Geophys. Res. Atmos.*, 121(21), 13,13-50,65,
523 doi:10.1002/2016JD025136, 2016.

524 Yarwood, G., Rao, S., Yocke, M. and Whitten, G. Z.: Updates to the carbon bond chemical mechanism: CB05, Final Rep. to
525 US EPA, RT-0400675, 8, 2005.

526 Yu, H., Dai, W., Ren, L., Liu, D., Yan, X., Xiao, H., He, J. and Xu, H.: The effect of emission control on the submicron
527 particulate matter size distribution in Hangzhou during the 2016 G20 Summit, *Aerosol Air Qual. Res.*, 18, 2038–2046, 2018.

528 Yu, S., Mathur, R., Pleim, J., Wong, D., Gilliam, R., Alapaty, K., Zhao, C. and Liu, X.: Aerosol indirect effect on the grid-
529 scale clouds in the two-way coupled WRF-CMAQ: model description, development, evaluation and regional analysis,
530 *Atmos. Chem. Phys. Discuss.*, 25649, 2013.

531 Zhai, S., Jacob, D. J., Wang, X., Shen, L., Li, K., Zhang, Y., Gui, K., Zhao, T. and Liao, H.: Fine particulate matter (PM_{2.5})
532 trends in China, 2013–2018: separating contributions from anthropogenic emissions and meteorology, *Atmos. Chem. Phys.*,
533 19(16), 11031–11041, doi:10.5194/acp-19-11031-2019, 2019.

534 Zhang, L., Shao, J., Lu, X., Zhao, Y., Hu, Y., Henze, D. K., Liao, H., Gong, S. and Zhang, Q.: Sources and processes
535 affecting fine particulate matter pollution over North China: an adjoint analysis of the Beijing APEC period, *Environ. Sci.*
536 *Technol.*, 50(16), 8731–8740, 2016.

537 Zhang, Q., He, K. and Huo, H.: Policy: cleaning China’s air, *Nature*, 484(7393), 161, 2012.

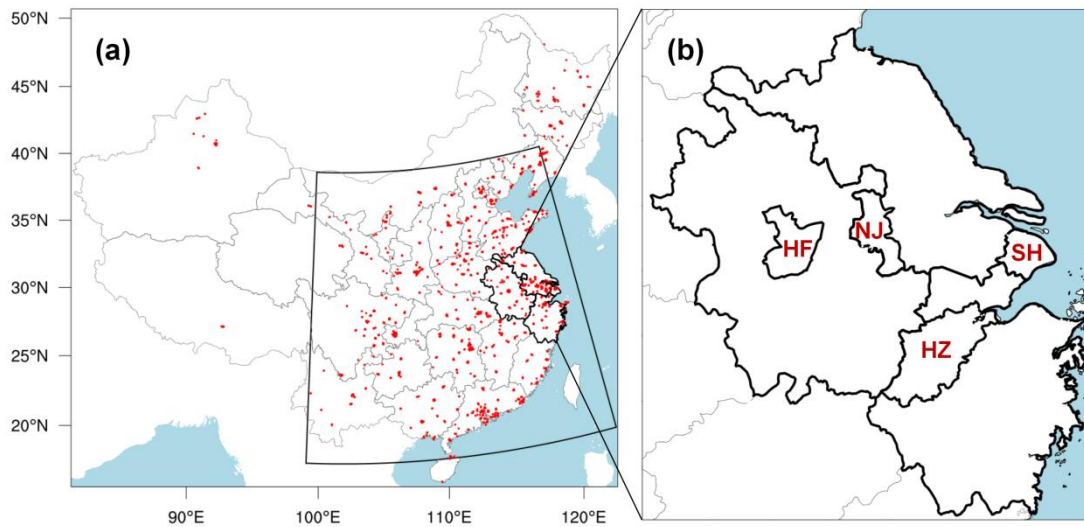
538 Zhang, Q., Zheng, Y., Tong, D., Shao, M., Wang, S., Zhang, Y., Xu, X., Wang, J., He, H., Liu, W. and others: Drivers of
539 improved PM_{2.5} air quality in China from 2013 to 2017, *Proc. Natl. Acad. Sci.*, 2019.

540 Zhang, R., Wang, G., Guo, S., Zamora, M. L., Ying, Q., Lin, Y., Wang, W., Hu, M. and Wang, Y.: Formation of urban fine
541 particulate matter, *Chem. Rev.*, 115(10), 3803–3855, 2015.

542 Zhang, Y.-L. and Cao, F.: Fine particulate matter (PM_{2.5}) in China at a city level, *Sci. Rep.*, 5, 14884, 2015.

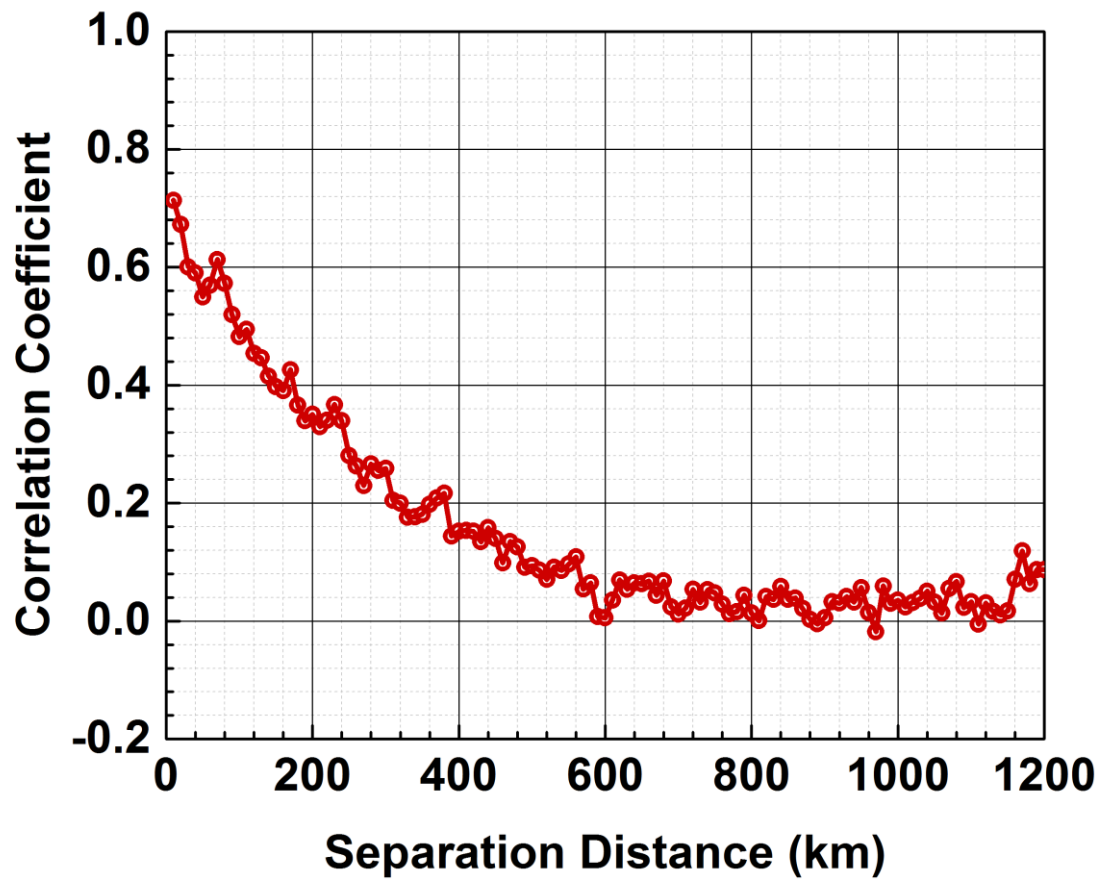
543 Zhong, Q., Ma, J., Shen, G., Shen, H., Zhu, X., Yun, X., Meng, W., Cheng, H., Liu, J., Li, B., Wang, X., Zeng, E. Y., Guan,
544 D. and Tao, S.: Distinguishing Emission-Associated Ambient Air PM_{2.5} Concentrations and Meteorological Factor-Induced
545 Fluctuations, *Environ. Sci. Technol.*, 52(18), 10416–10425, doi:10.1021/acs.est.8b02685, 2018.

546



497
 498
 499
 500
 501
 502
 503
 504
 505
 506
 507
 508
 509
 510

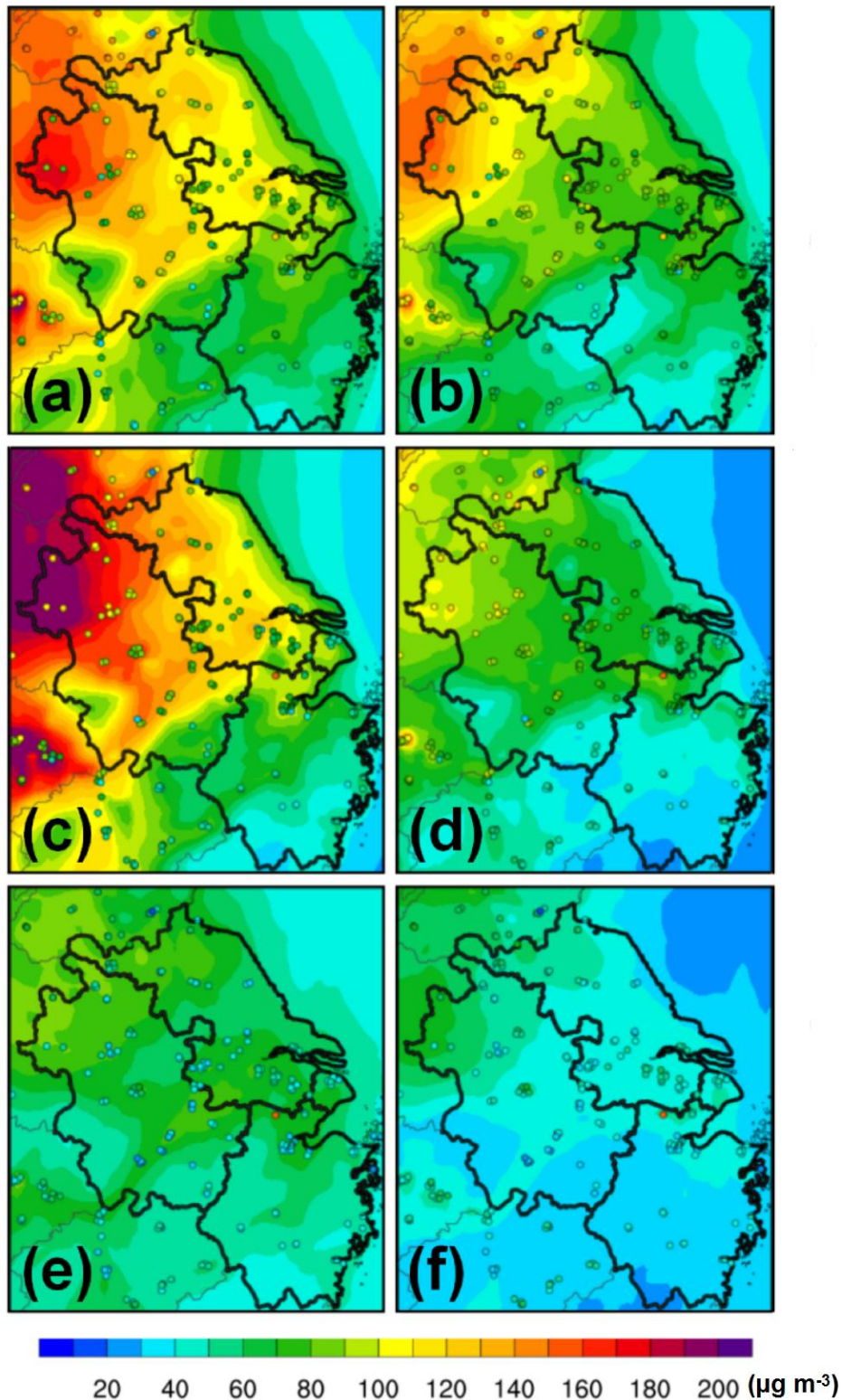
Figure 1. (a) The model domain. Red dots denote the ground-level PM_{2.5} measurements, which, within the fan-shaped quadrilateral, are used to constrain the model predictions. (b) Black lines outline the boundaries of the Yangtze River Delta (YRD), as well as four major cities considered (i.e., SH: Shanghai; HZ: Hangzhou; NJ: Nanjing; HF: Hefei).



511

512 Figure 2. Correlation coefficients (averaged over 10 km) as a function of the separation distances between two
513 surface-level monitoring stations using the Hollingsworth-Lönnerberg method.

514



515

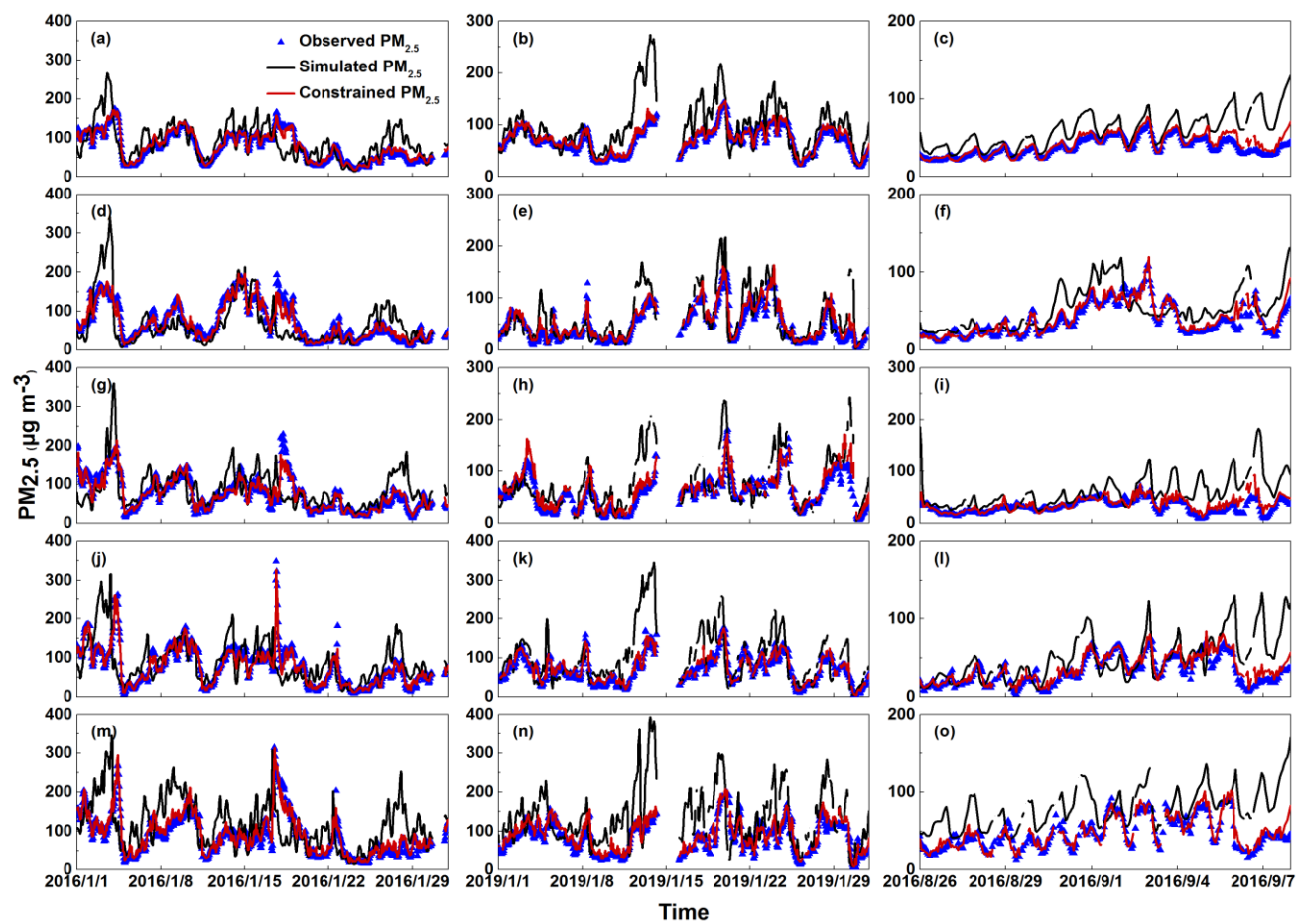
516

517

518

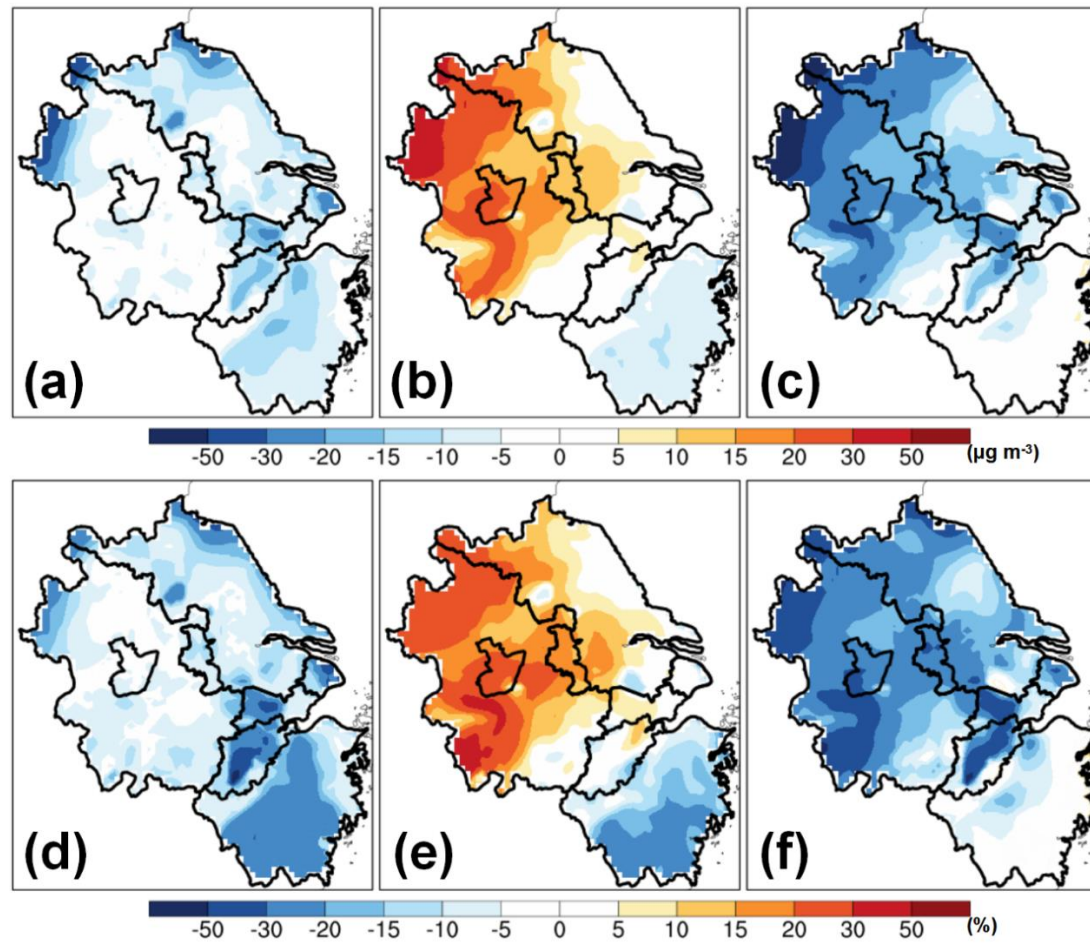
519

Figure 3. Spatial comparisons of hourly-averaged concentrations of simulated and constrained $\text{PM}_{2.5}$ with surface observations across the YRD for January 2016 (top panel), January 2019 (middle panel), and the G20 summit (bottom panel): (a) NO_2016; (b) DA_2016; (c) NO_2019; (d) DA_2019; (e) NO_G20; (f) DA_G20. Circles denote ground measurement sites.



520

521 Figure 4. Time series of the comparisons between hourly observed, simulated, and constrained $PM_{2.5}$ concentrations for January 2016 (left column), January 2019 (middle column),
 522 and the G20 summit (right column) over (a – c) the whole domain as well as in four representative cities, which are as follows: (d - f) Shanghai, (g - i) Hangzhou, (j - l) Nanjing, and (m
 523 - o) Hefei. The black circles, black lines, and red lines denote the hourly observed, simulated, and constrained $PM_{2.5}$ concentrations, respectively.

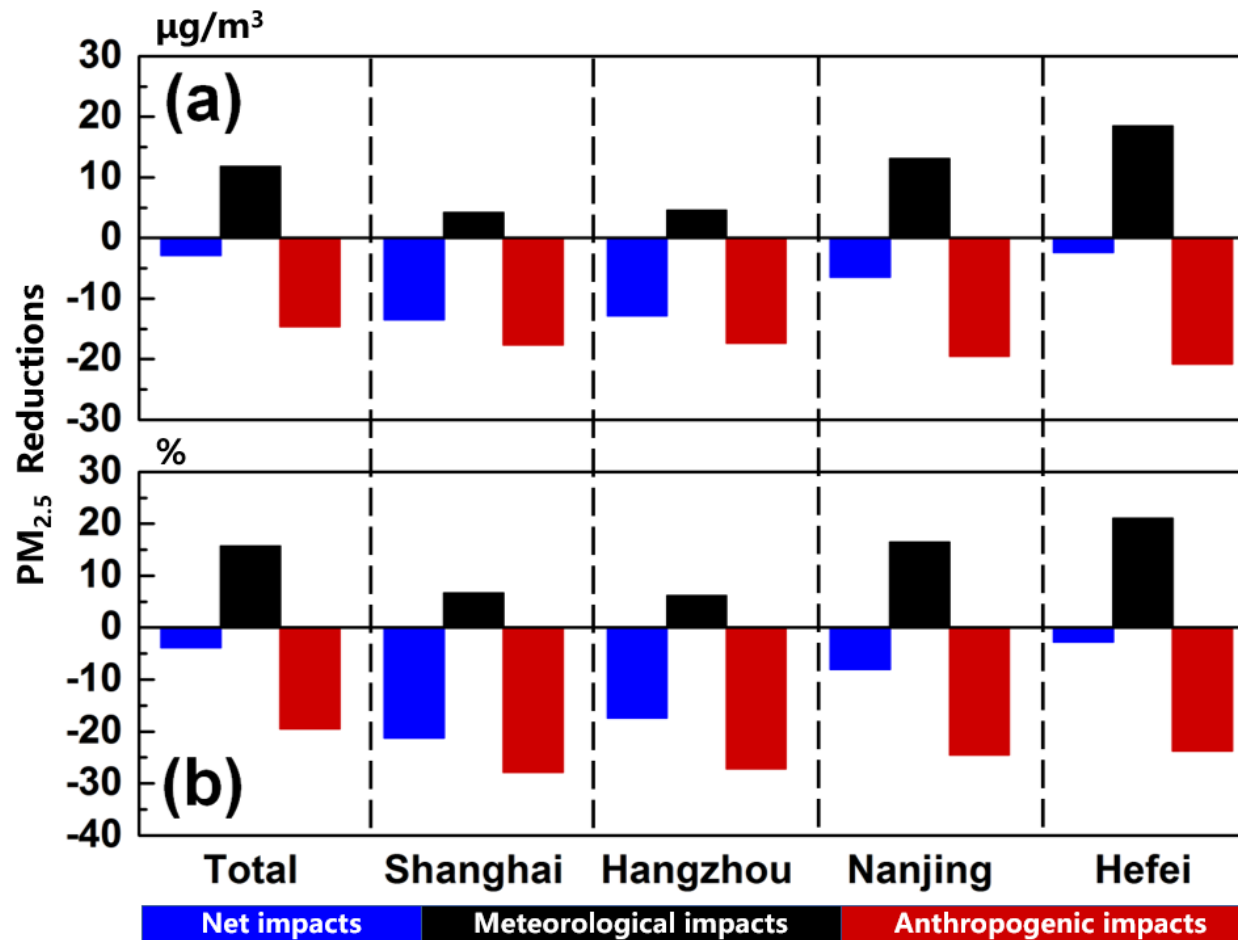


524

525

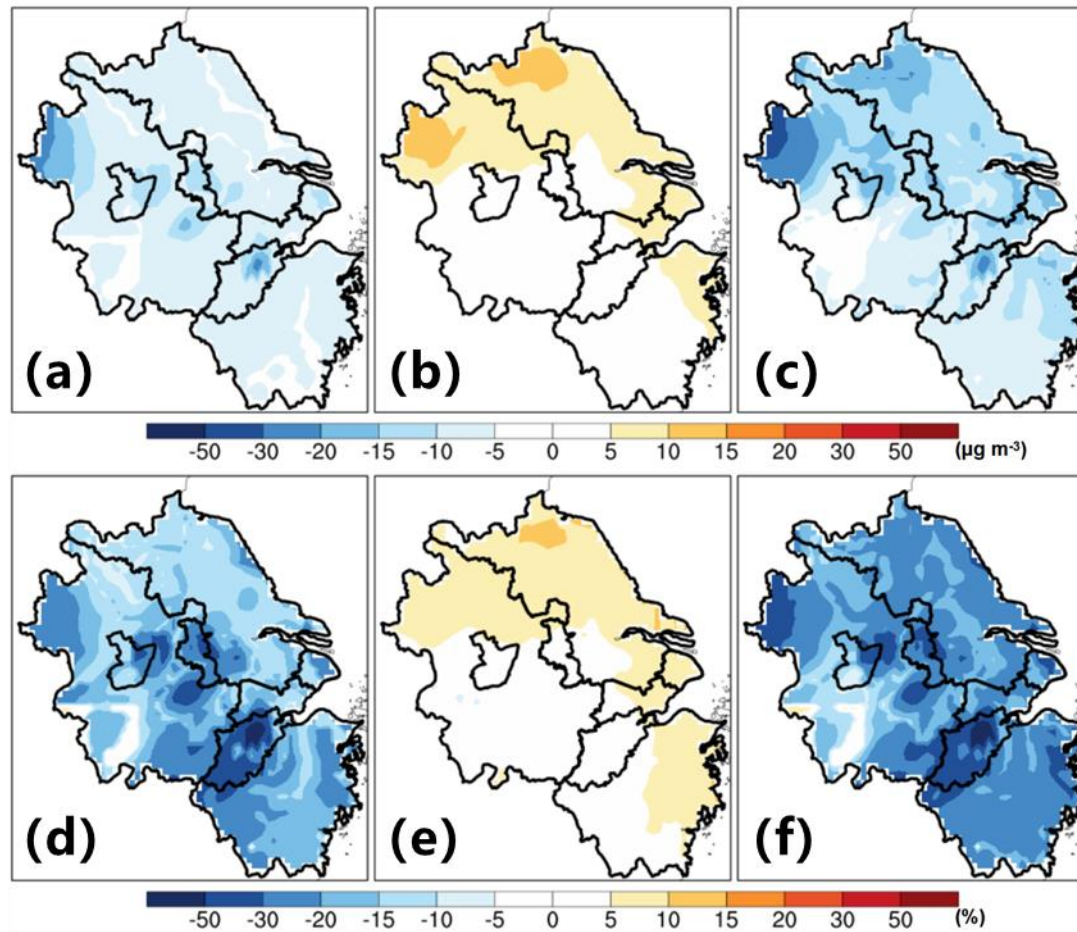
526

Figure 5. The impacts of anthropogenic emission controls and meteorological variations on spatial PM_{2.5} concentrations in January from 2016 to 2019. (a, d) Their net impacts. (b, e) meteorological impacts. (c, f) the impacts of anthropogenic emission controls. The top and bottom panels refer to the changes in absolute values and relative percentages, respectively.



527

528 Figure 6. The impacts of anthropogenic emission controls and meteorological variations on PM_{2.5} concentrations in January from 2016 to 2019 over the whole domain as well as in four
 529 representative cities (i.e., Shanghai, Hangzhou, Nanjing, and Hefei). The top and bottom panels refer to the changes in absolute values and relative percentages, respectively.



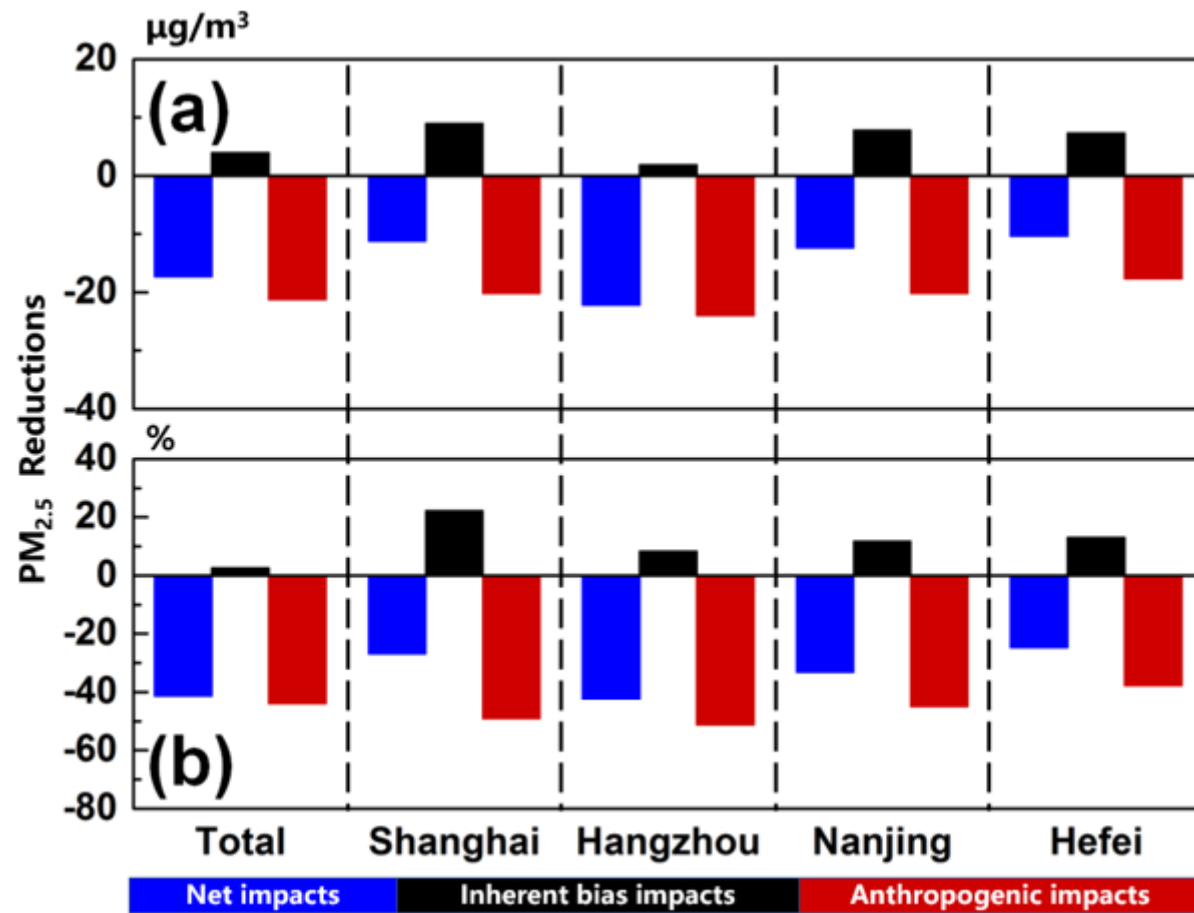
530

531

532

533

Figure 7. The impacts of anthropogenic emission controls and inherent biases on spatial PM_{2.5} concentrations during the G20 summit. (a, d) Their net impacts. (b, e) the impacts of inherent biases. (c, f) the impacts of anthropogenic emission controls. The top and bottom panels refer to the changes in absolute values and relative percentages, respectively. Inherent biases are mainly due to the prior anthropogenic emissions.



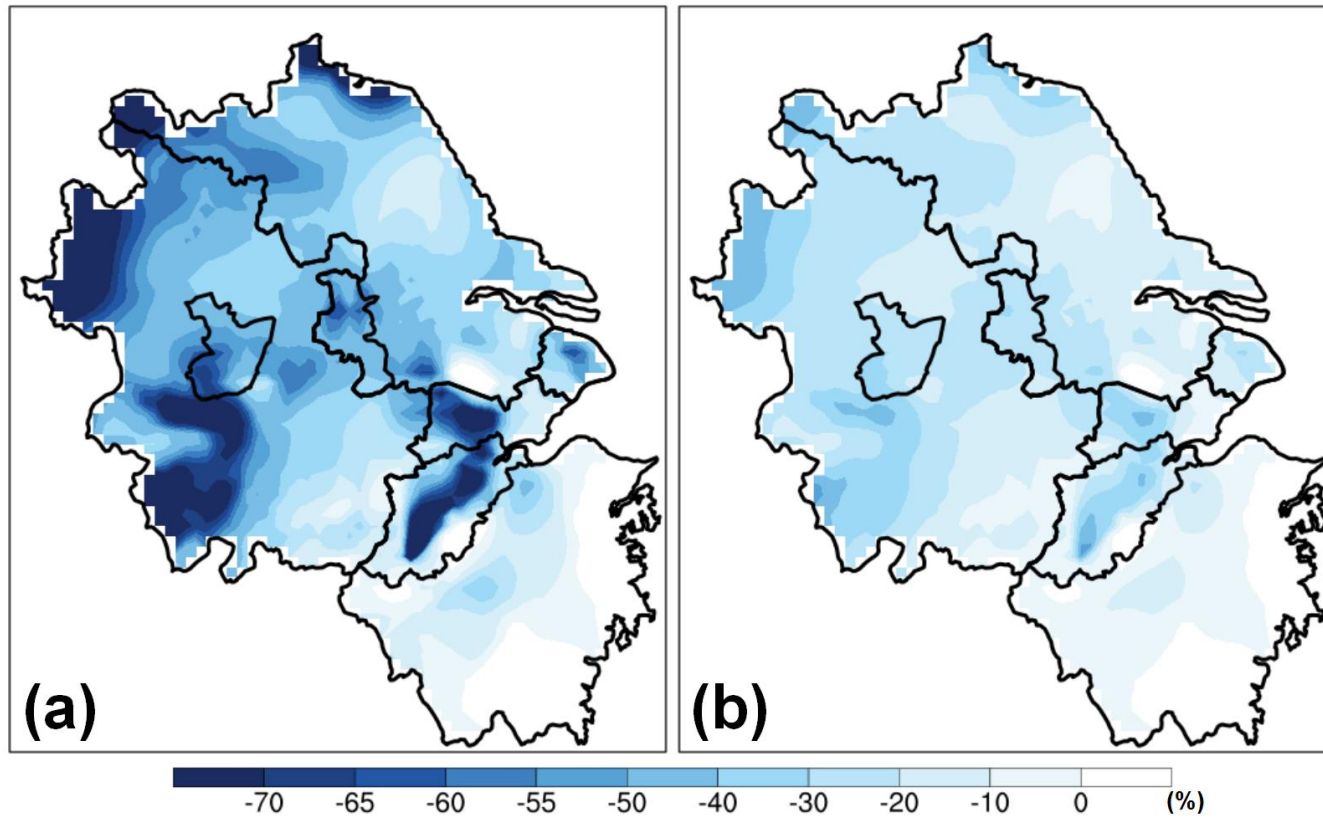
534

535

536

537

Figure 8. The impacts of anthropogenic emission controls and inherent biases on PM_{2.5} concentrations during the G20 summit over the whole domain as well as in four representative cities (i.e., Shanghai, Hangzhou, Nanjing, and Hefei). The top and bottom panels refer to the changes in absolute values and relative percentages, respectively. Inherent biases are mainly due to the prior anthropogenic emissions.



538

539 **Figure 9. (a) Spatial distributions of the PM_{2.5} mitigation potential across the YRD and (b) their differences with the impacts of long-term emission control strategies from 2016 to 2019**
540 **(Fig. 5f). Both spatial patterns of long-term emission control strategy impacts (Fig. 5f) and the localized PM_{2.5} mitigation potential in the main urban areas of Hangzhou (Fig. S10), with**
541 **the proportion calculator, result in Fig. 9a.**

542

543

Table 1. The experiments to isolate the effects of anthropogenic emission controls due to the long-term and emergency emission control strategies.

Experiments	Time Periods	Priori Anthropogenic Emissions	Constrained Meteorology	Constrained Observations	Comparisons and Purposes
DA_2016	January 2016	MEICv1.2	Yes	Yes	The net effects of major driving factors (i.e., anthropogenic emission controls and meteorological variations) from 2016 to 2019.
DA_2019	January 2019		Yes	Yes	
NO_2016	January 2016	MEICv1.2	Yes	No	The effects of meteorological variations from 2016 to 2019.
NO_2019	January 2019		Yes	No	
DA_G20	from August 26 to	MEICv1.2	Yes	Yes	The net effects of major driving factors (i.e., anthropogenic emission controls and the uncertainties in the priori anthropogenic emissions) during the G20 summit.
NO_G20	September 7, 2016		Yes	No	
DA_CON_G20	from August 11 to	MEICv1.2	Yes	Yes	The effects of the uncertainties in the priori anthropogenic emissions.
NO_CON_G20	August 23 and from September 18 to September 30, 2016		Yes	No	

Supporting Information for Significant PM_{2.5} mitigation in the Yangtze River Delta, China: observational constraints on surface PM_{2.5} responses to anthropogenic emission controls from 2016 to 2019

Liqiang Wang¹, Shaocai Yu^{*,1,2}, Pengfei Li^{*,3,1}, Xue Chen¹, Zhen Li¹, Yibo Zhang¹, Mengying Li¹, Khalid Mehmood¹, Weiping Liu¹, Tianfeng Chai⁴, Yannian Zhu⁵, Daniel Rosenfeld⁶, and John H. Seinfeld²

¹Research Center for Air Pollution and Health; Key Laboratory of Environmental Remediation and Ecological Health, Ministry of Education, College of Environment and Resource Sciences, Zhejiang University, Hangzhou, Zhejiang 310058, P.R. China

²Division of Chemistry and Chemical Engineering, California Institute of Technology, Pasadena, CA 91125, USA

³College of Science and Technology, Hebei Agricultural University, Baoding, Hebei 071000, P.R. China

⁴Air Resources Laboratory, NOAA, Cooperative Institute for Satellite Earth System Studies (CISESS), University of Maryland, College Park, USA

⁵Meteorological Institute of Shanxi Province, 36 Beiguangzhengjie, Xi'an 710015, China

⁶Institute of Earth Science, The Hebrew University of Jerusalem, Jerusalem, Israel

Correspondence to: Shaocai Yu (shaocaiyu@zju.edu.cn); Pengfei Li (lpf_zju@163.com)

Content:

Figure S1. Meteorological factors during the G20 summit and its adjacent period.

Figure S2. The NMB and R values of the simulated and constrained PM_{2.5}.

Figure S3. The NMB values and their standard deviations of the simulated and constrained PM_{2.5} on the basis of four intervals of the observations.

Figure S4. The NMB values and their standard deviations of the simulated and constrained PM_{2.5} at the 24-hour scale.

Figure S5. Time series of the observed and constrained temperature.

Figure S6. Time series of the observed and constrained relative humidity.

Figure S7. Time series of the observed and constrained wind speed.

Figure S8. Time series of the observed and constrained air pressure.

Figure S9. Spatial distributions of the monthly anthropogenic emissions.

Figure S10. Impacts of different emissions on the meteorology.

Figure S11. Standard deviations of the impacts of inherent biases.

Figure S12. The enlarged part in Figure 7c.

Table S1. Evaluation statistics of the constrained PM_{2.5}.

Table S2. Evaluation statistics of the constrained temperature.

Table S3. Evaluation statistics of the constrained relative humidity.

Table S4. Evaluation statistics of the constrained wind speed.

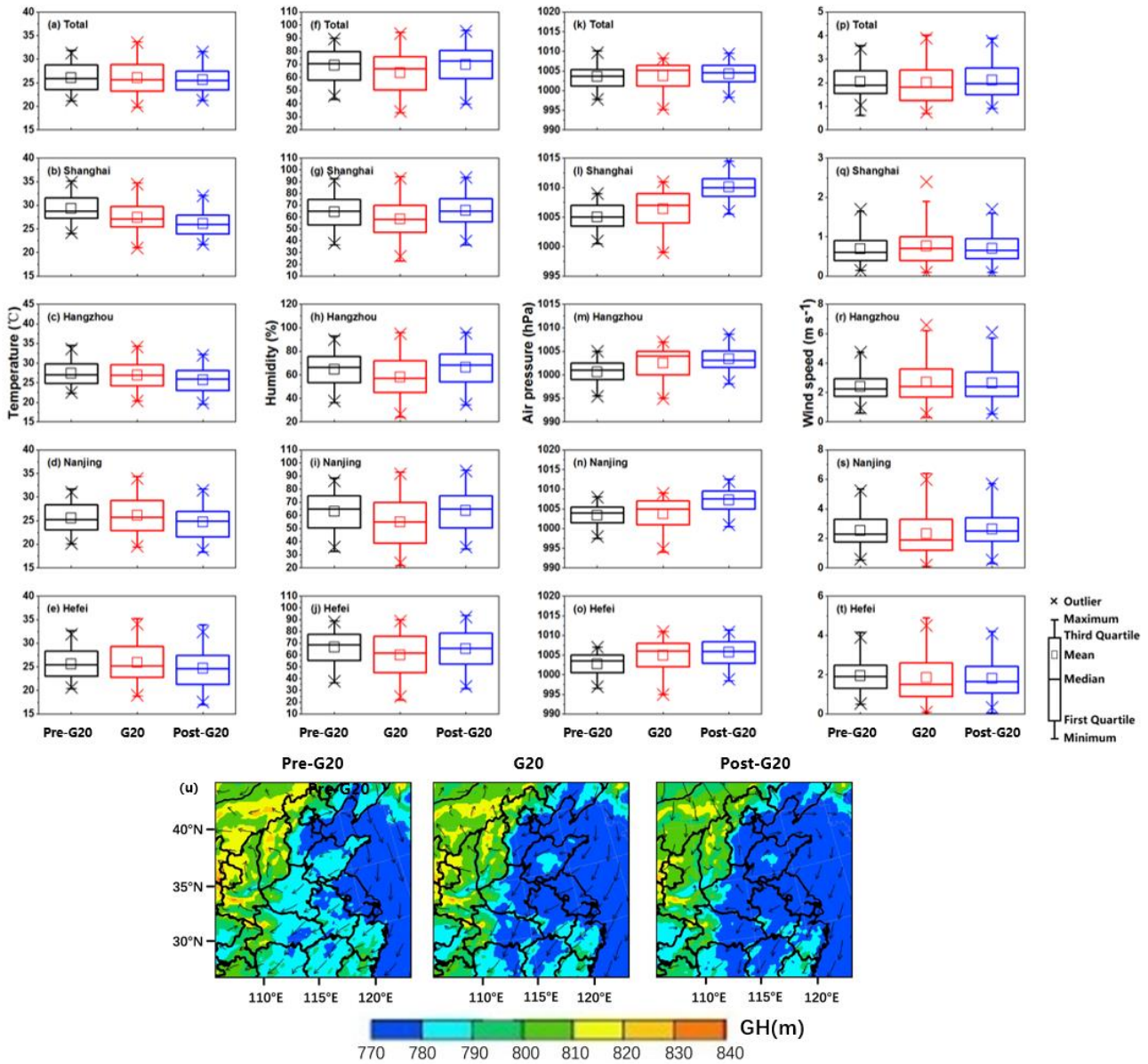
Table S5. Evaluation statistics of the constrained air pressure.

Table S6. Different effects between the long-term emission controls and the emergency emission controls.

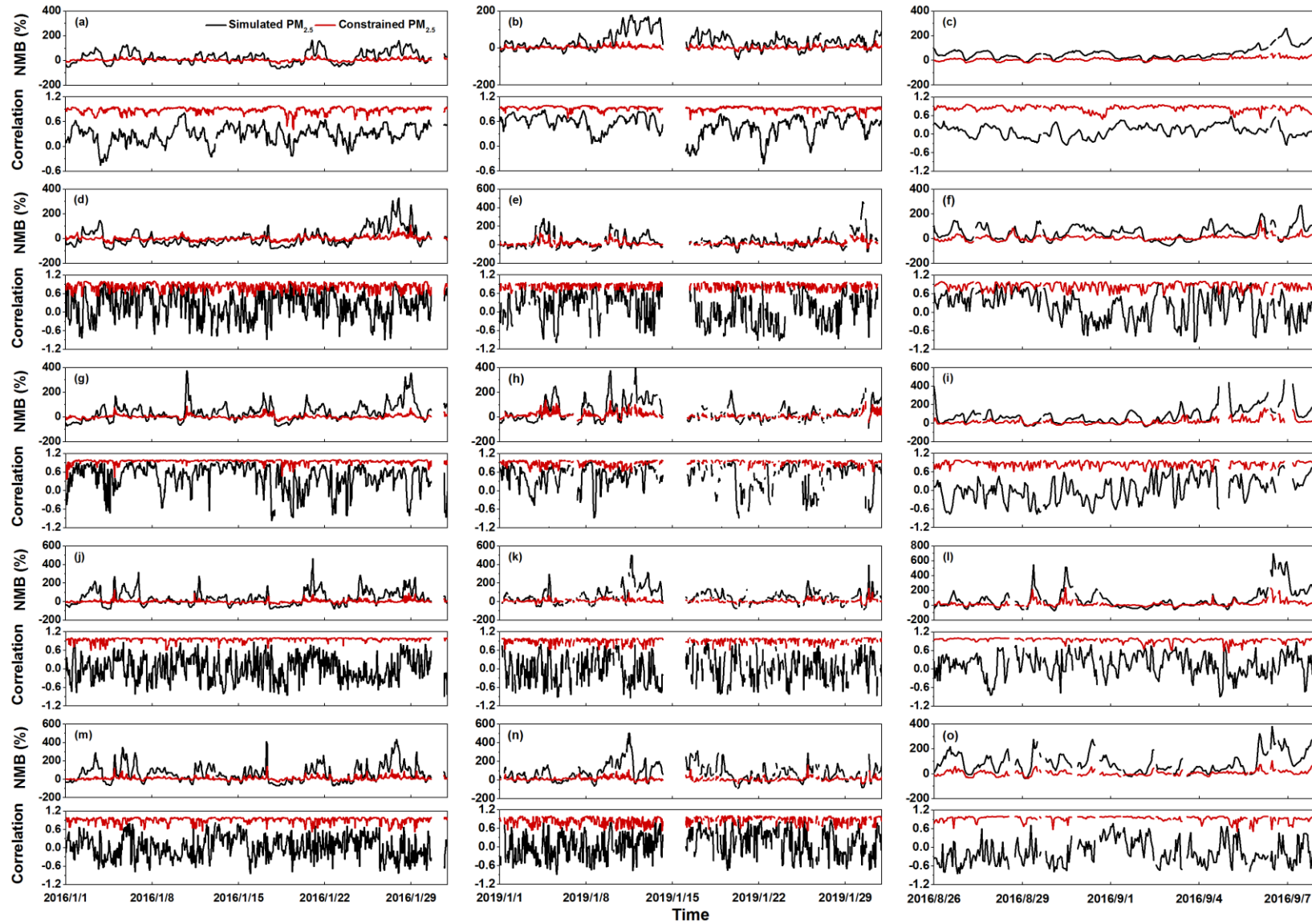
No. of Pages: 19

No. of Figures: 12

No. of Tables: 6

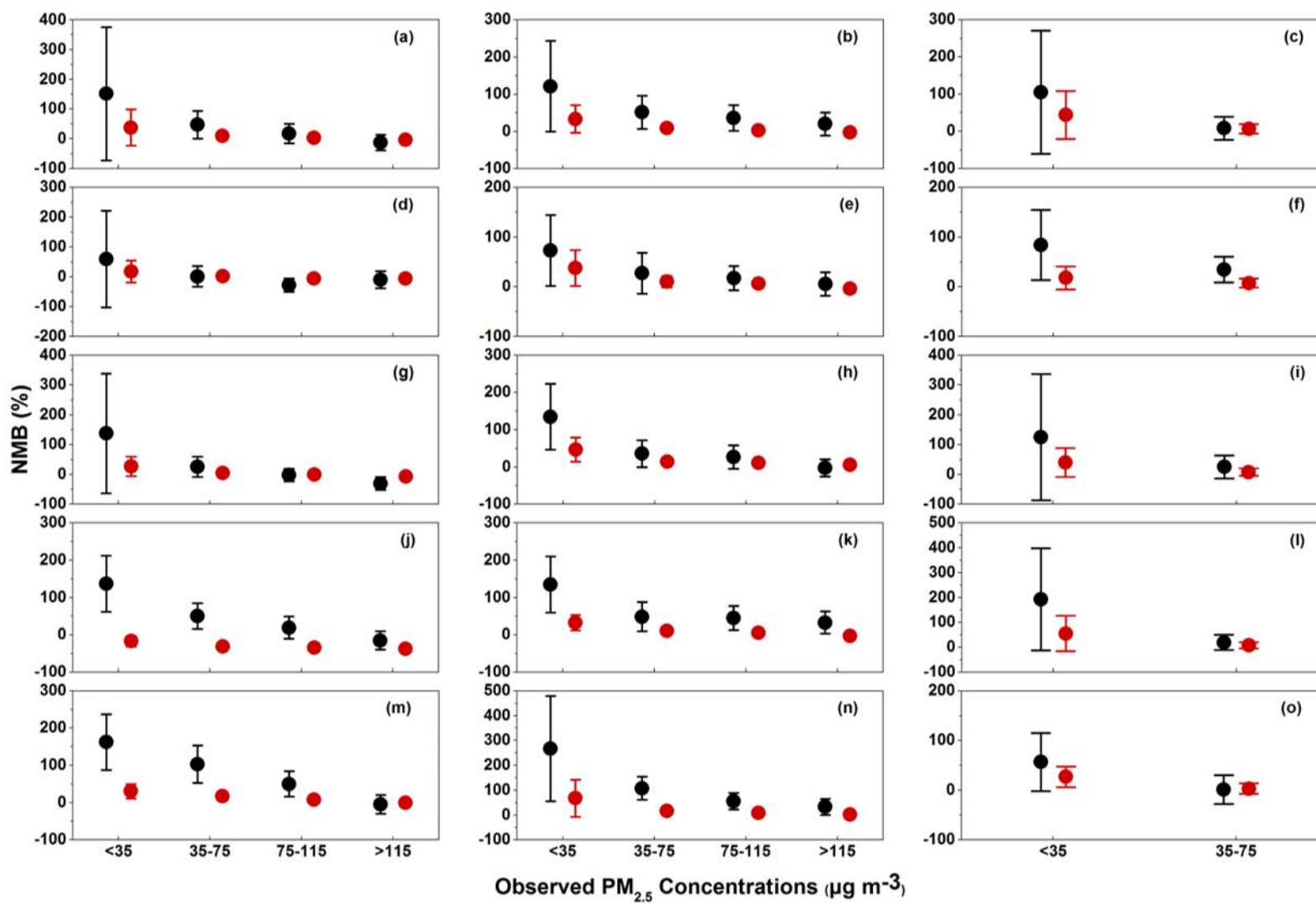


41
 42 **Figure S1. (a - t) The reanalysed meteorological factors (i.e., temperature, relative humidity, air pressure, and wind speed) at four**
 43 **cities during the G20 summit and its adjacent periods (i.e., Pre- and Post- G20 periods, from August 11 to August 23, 2016 and from**
 44 **September 18 to September 30, 2016, respectively) and (u) the corresponding atmospheric synoptic circulation patterns at at**
 45 **925 hPa (the geopotential height (GH) fields (colored shading) and wind vector fields (arrows)).**



46
47
48

Figure S2. The NMB and R values of the simulated (black) and constrained (red) hourly $PM_{2.5}$ concentrations for January 2016 (left column), January 2019 (middle column), and the G20 summit (right column) over the whole domain (a - c) as well as in four representative cities, which are as follows: Shanghai (d - f), Hangzhou (g - i), Nanjing (j - l), and Anhui (m - o).



49

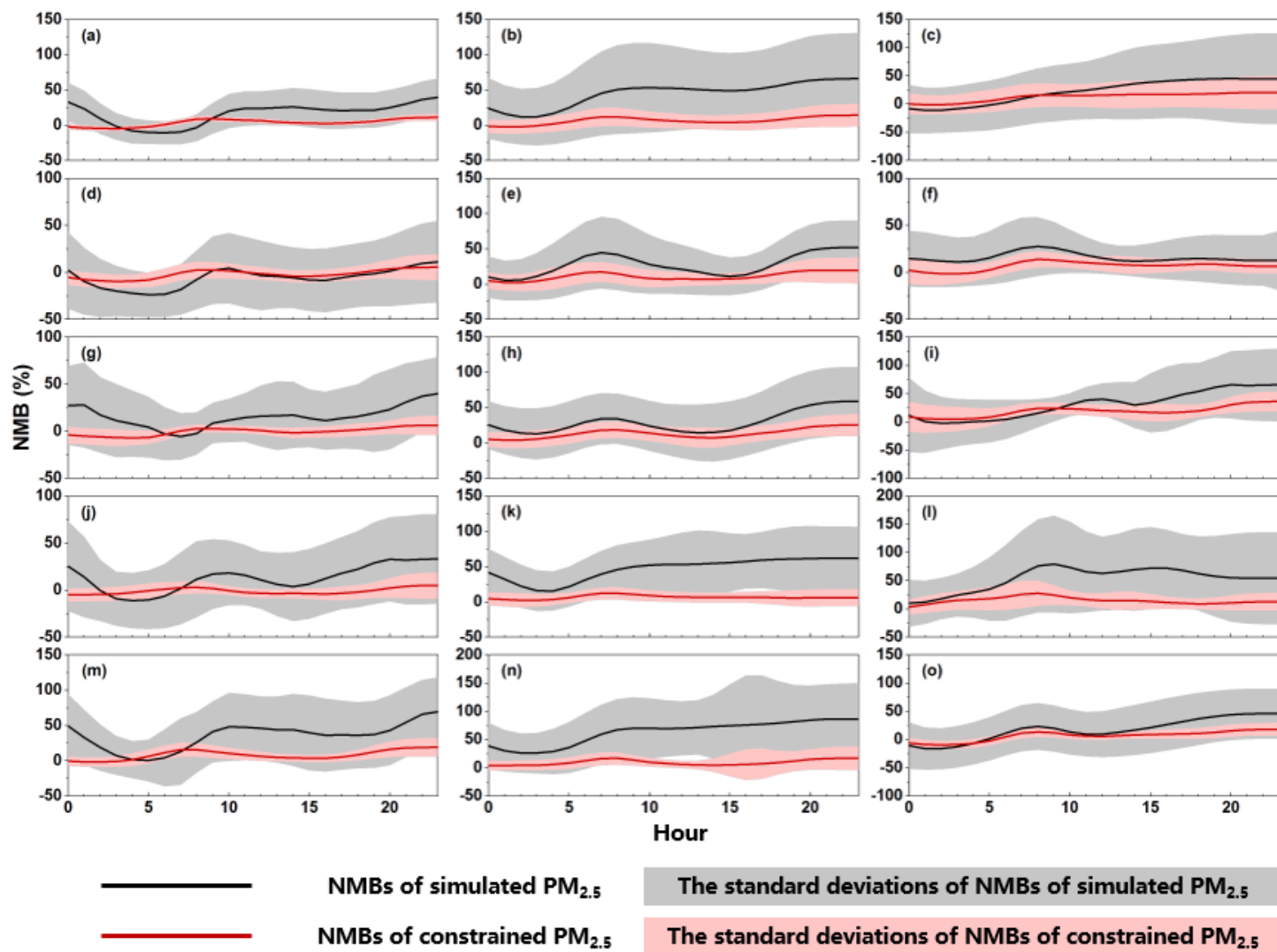
50

Figure S3. The mean NMB values (dots) and their standard deviations (bars) of the simulated (black) and constrained (red) hourly $PM_{2.5}$ concentrations on the basis of four intervals of the observations during January 2016 (left column), January 2019 (middle column), and the G20 summit (right column) over the whole domain (a - c) as well as in four representative cities, which are as follows:

51

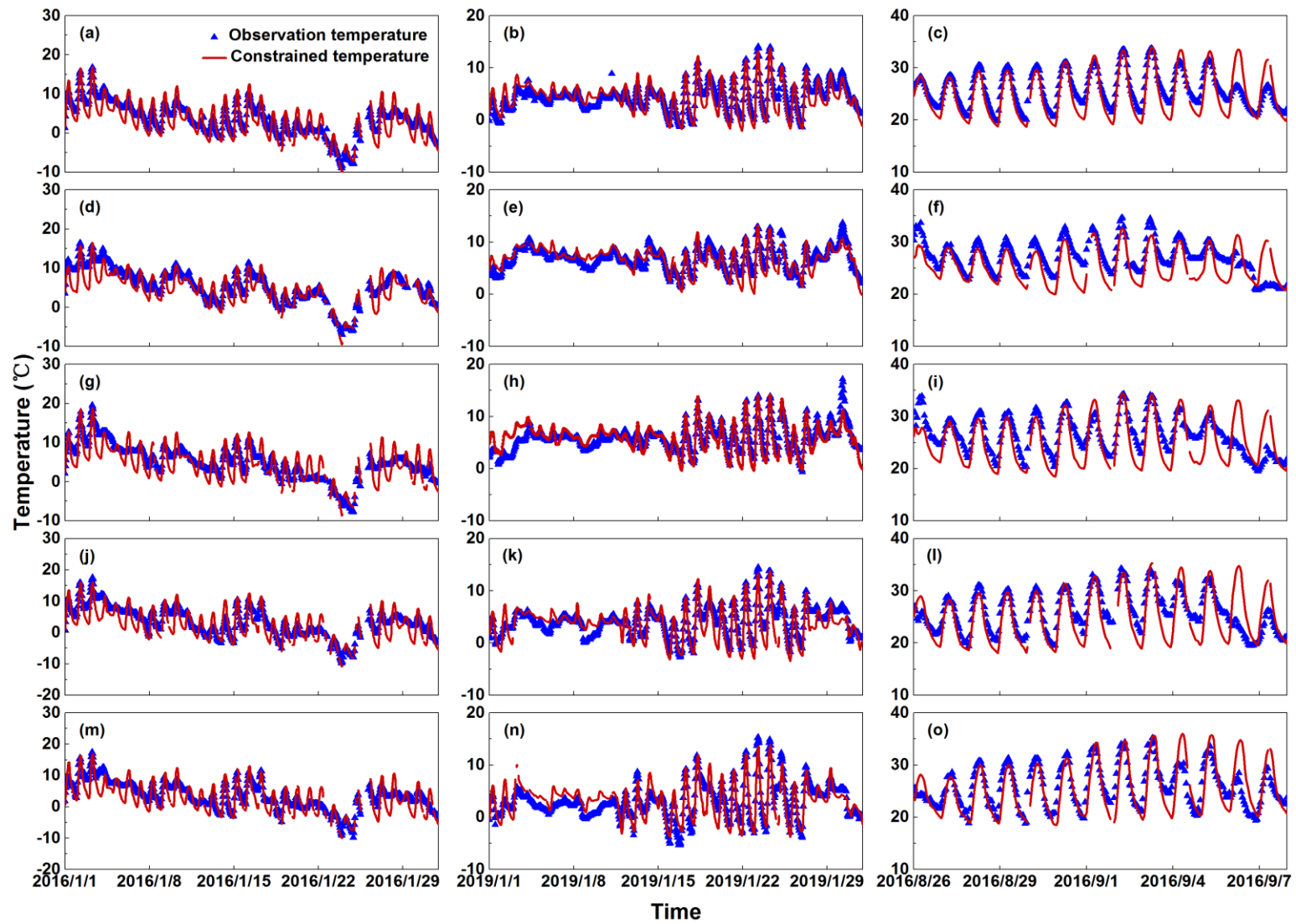
Shanghai (d - f), Hangzhou (g - i), Nanjing (j - l), and Anhui (m - o).

52



53
54
55
56

Figure S4. Time series of the mean NMB values and their standard deviations of the simulated and constrained hourly $PM_{2.5}$ concentrations for January 2016 (left column), January 2019 (middle column), and the G20 summit (right column) over the whole domain (a - c) as well as in four representative cities, which are as follows: Shanghai (d - f), Hangzhou (g - i), Nanjing (j - l), and Anhui (m - o).



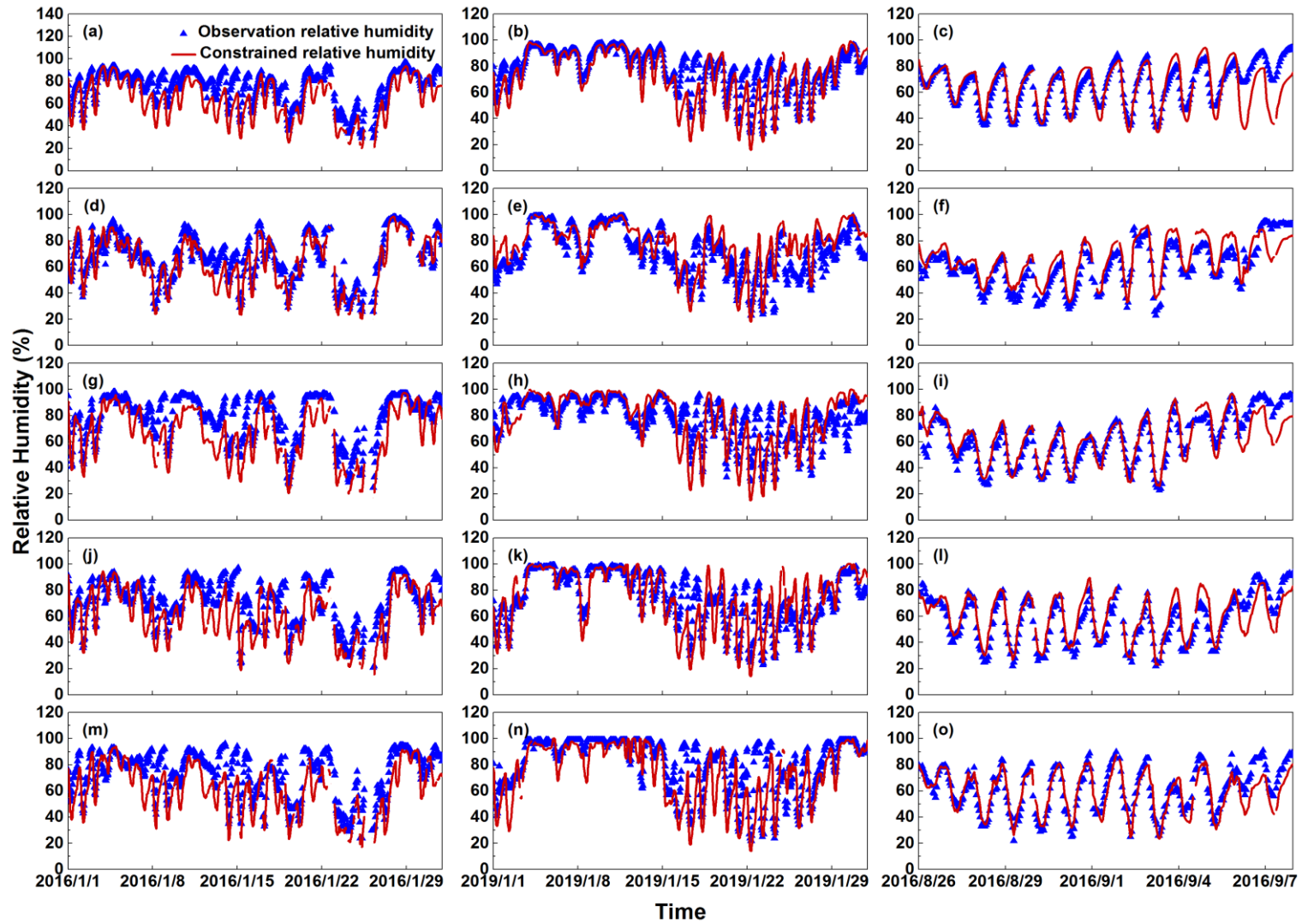
57

58

Figure S5. Time series of the hourly observed and constrained temperature for January 2016 (left column), January 2019 (middle column), and the G20 summit (right column) over the whole domain

59

(a - c) as well as in four representative cities, which are as follows: Shanghai (d - f), Hangzhou (g - i), Nanjing (j - l), and Anhui (m - o).

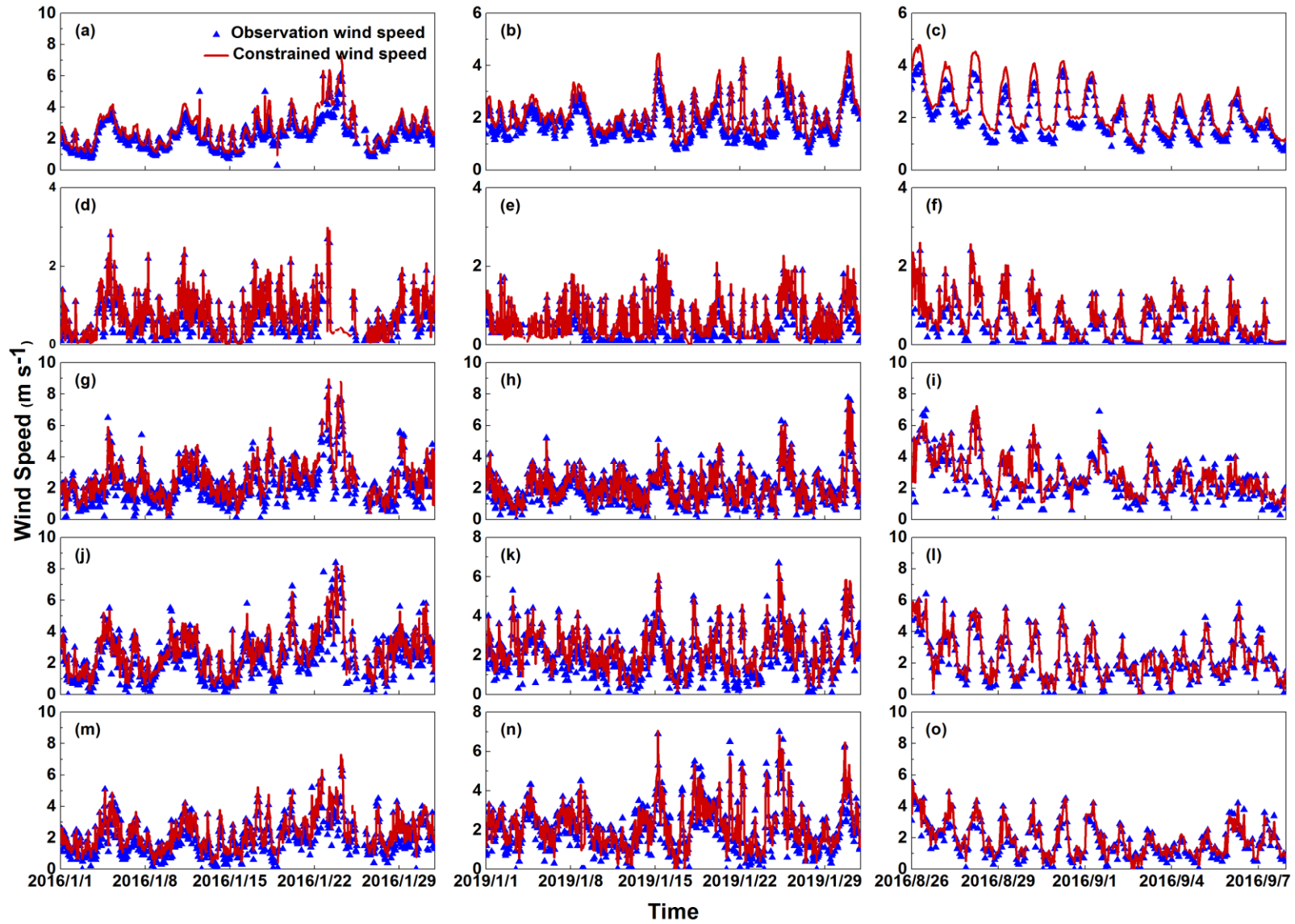


60

61

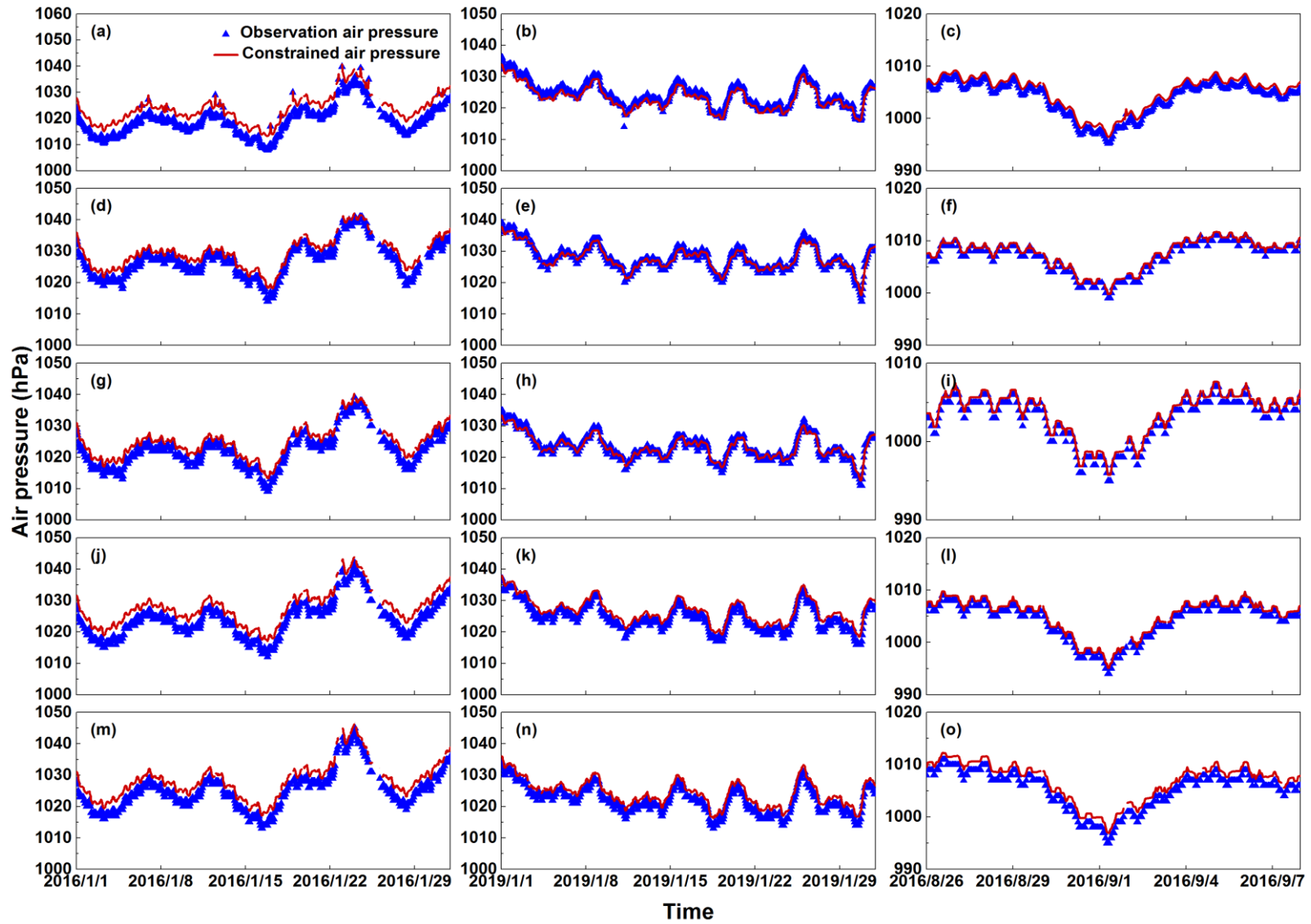
62

Figure S6. Time series of the comparisons between hourly observed and constrained relative humidity for January 2016 (left column), January 2019 (middle column), and the G20 summit (right column) over the whole domain (a - c) as well as in four representative cities, which are as follows: Shanghai (d - f), Hangzhou (g - i), Nanjing (j - l), and Anhui (m - o).



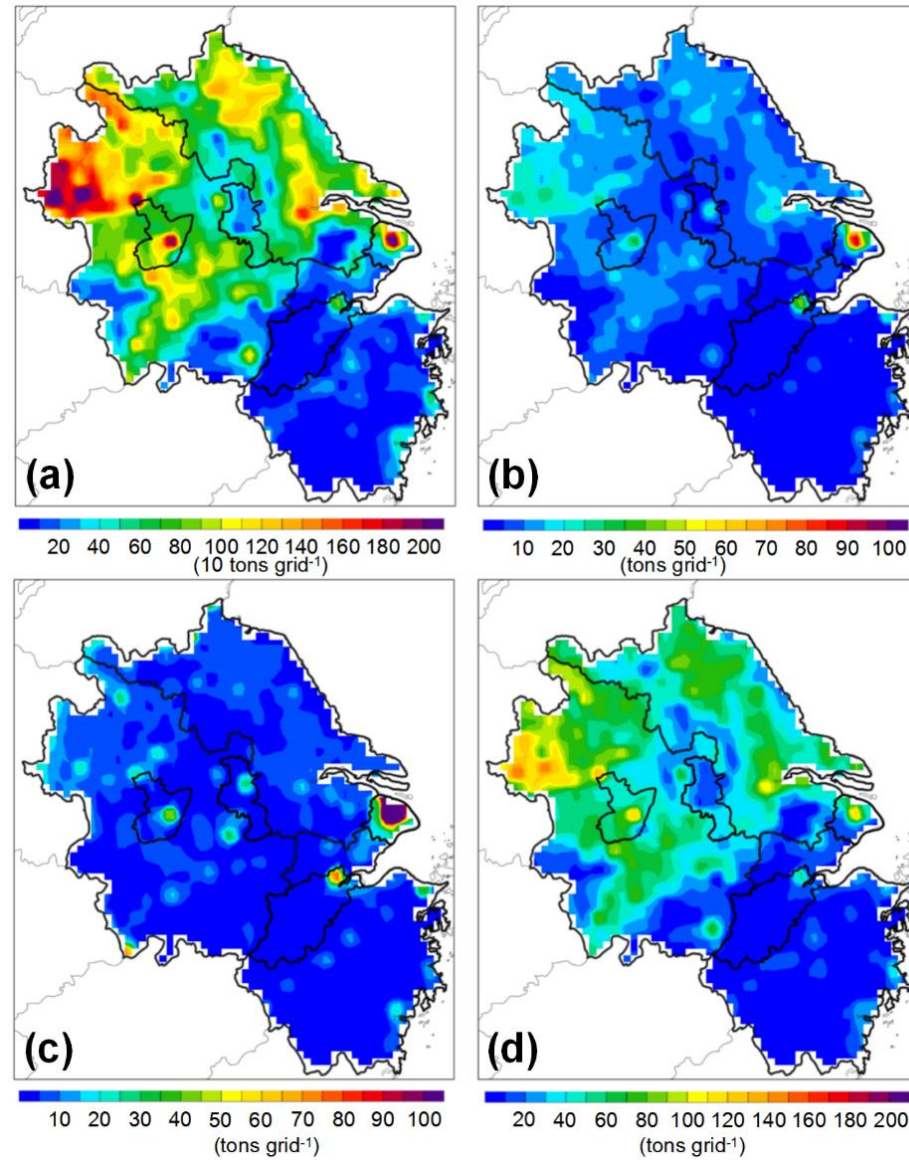
63
64
65

Figure S7. Time series of the comparisons between hourly observed and constrained wind speed for January 2016 (left column), January 2019 (middle column), and the G20 summit (right column) over the whole domain (a - c) as well as in four representative cities, which are as follows: Shanghai (d - f), Hangzhou (g - i), Nanjing (j - l), and Anhui (m - o).



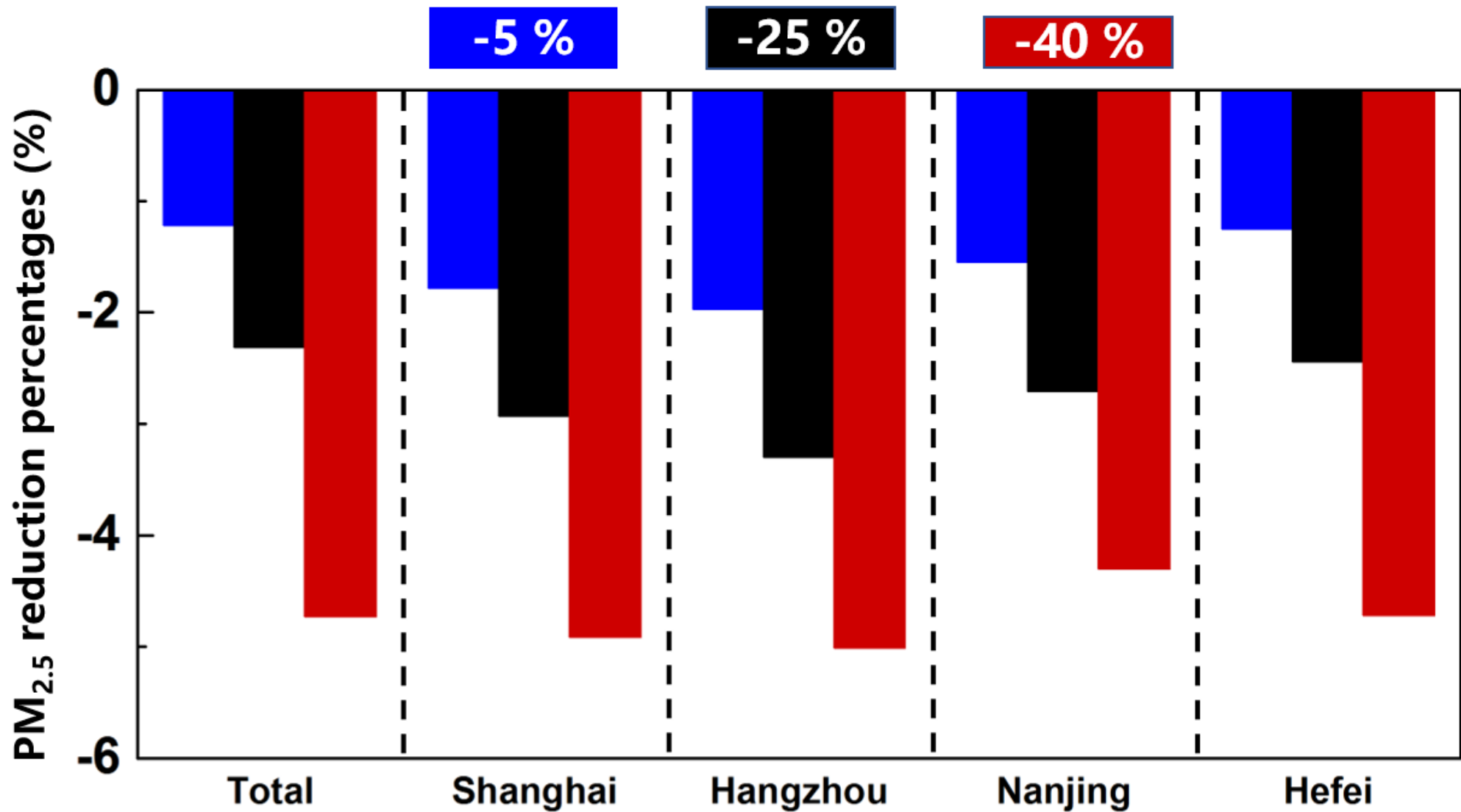
66

67 Figure S8. Time series of the comparisons between hourly observed and constrained air pressure for January 2016 (left column), January 2019 (middle column), and the G20 summit (right column)
 68 over the whole domain (a - c) as well as in four representative cities, which are as follows: Shanghai (d - f), Hangzhou (g - i), Nanjing (j - l), and Anhui (m - o).



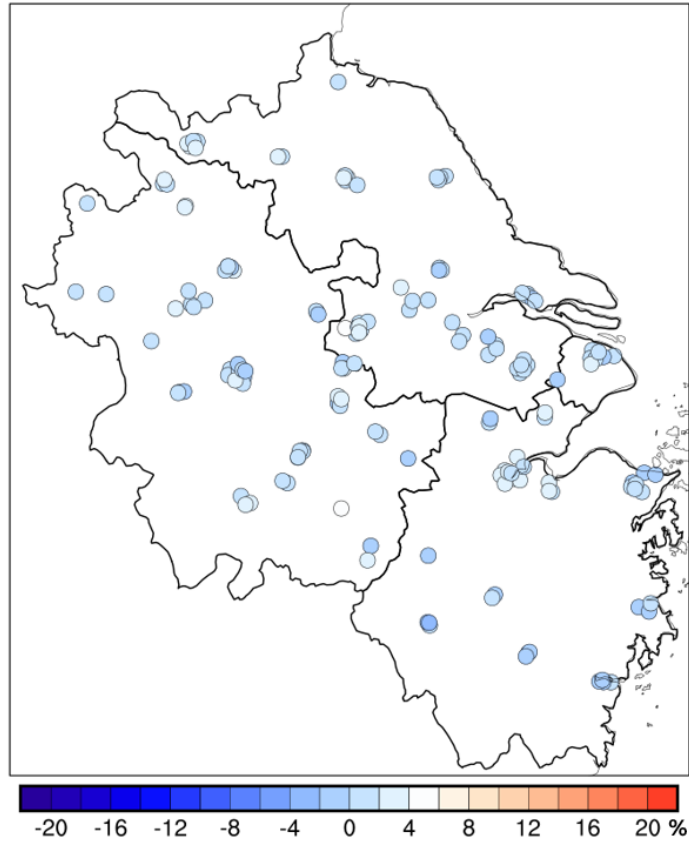
69

70 **Figure S9. Spatial distributions of the monthly emissions of (a) CO, (b) NO_x, (c) SO₂, and (d) PM_{2.5} in the prior anthropogenic emission inventory (MEICv1.2).**



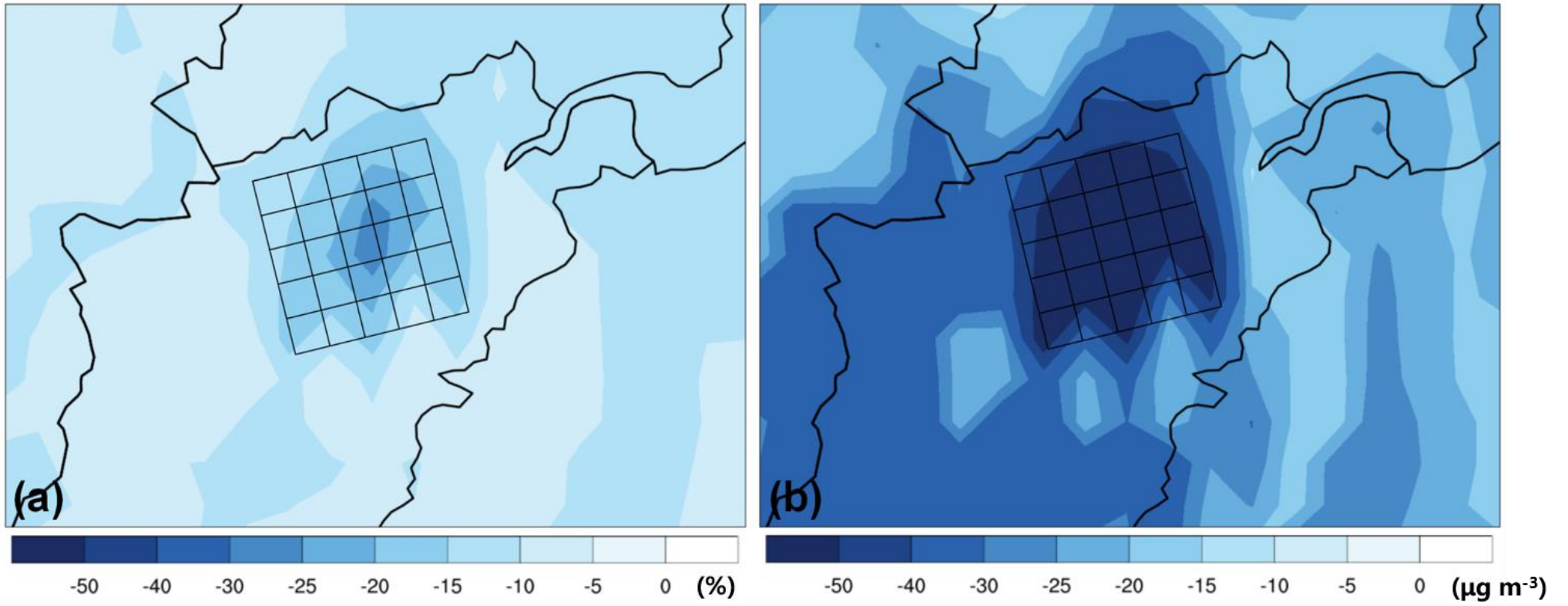
71
72
73

Figure S10. Meteorological impacts on PM_{2.5} concentrations in three sensitivity cases over the whole domain as well as in four representative cities, which are as follows: Shanghai, Hangzhou, Nanjing, and Anhui. The three corresponding adjustment coefficients are 5 %, 25 %, and 40 %, respectively.



74
75
76
77
78

Figure S11. Standard deviations of the impacts of the inherent biases during the adjacent periods of the G20 summit (i.e., pre- and post- periods, from August 11 to August 23, 2016 and from September 18 to September 30, 2016, respectively). The dots denote the locations of ground PM_{2.5} measurements.



79
80
81
82
83
84
85

Figure S12. The enlarged part in Figure 7c. The black fishnets mark the grids covering the areas with the ultimate PM_{2.5} mitigations, which are mostly located in urban Hangzhou.

Table S1. Comprehensive evaluation statistics of the constrained PM_{2.5} over the whole domain as well as in four representative cities as follows: Shanghai, Hangzhou, Nanjing, and Hefei.

Episode	Area	Observed	Constrained PM _{2.5}		NMB		RMSE		R	
		PM _{2.5}	(μg m ⁻³)		(%)		(μg m ⁻³)			
		(μg m ⁻³)	UNCONS	CONS	UNCONS	CONS	UNCONS	CONS	UNCONS	CONS
2016	Total	76.50	89.30	78.78	16.73	2.97	38.66	7.15	0.63	0.98
	Shanghai	70.40	66.30	68.94	-5.82	-2.07	46.36	11.66	0.65	0.97
	Hangzhou	75.05	86.84	74.39	15.70	-0.89	47.73	11.16	0.48	0.97
	Nanjing	79.57	89.60	78.01	12.61	-1.95	57.64	10.56	0.42	0.98
	Hefei	87.64	118.29	92.96	34.97	6.08	72.90	14.56	0.35	0.97
2019	Total	70.66	97.08	73.52	37.40	4.05	44.17	5.90	0.71	0.98
	Shanghai	48.77	62.66	54.21	28.47	11.14	34.05	10.38	0.75	0.97
	Hangzhou	59.65	78.55	67.75	31.70	13.59	43.24	14.41	0.65	0.95
	Nanjing	71.32	104.67	75.36	46.75	5.67	62.24	10.11	0.66	0.97
	Hefei	85.29	136.71	92.69	60.30	8.68	80.88	14.36	0.52	0.95
G20	Total	38.05	59.31	41.99	55.89	10.35	27.74	6.60	0.59	0.93
	Shanghai	38.91	52.73	41.56	35.49	6.80	25.77	7.43	0.60	0.95
	Hangzhou	32.05	59.39	37.25	85.29	16.20	39.60	9.92	0.33	0.79
	Nanjing	33.18	49.60	37.26	49.50	12.31	31.83	8.18	0.41	0.92
	Hefei	47.05	79.53	49.18	69.01	4.53	40.99	8.53	0.40	0.92

Table S2. Comprehensive evaluation statistics of the constrained temperature over the whole domain as well as in four representative cities as follows: Shanghai, Hangzhou, Nanjing, and Hefei.

Episode	Area	Observations (□)	Constrained temperature (□)	NMB (%)	RMSE (□)	R
2016	Total	3.67	3.09	-15.80	2.19	0.89
	Shanghai	5.67	4.55	-19.82	2.30	0.89
	Hangzhou	5.25	4.48	-14.75	2.77	0.83
	Nanjing	3.51	2.45	-30.31	2.94	0.84
	Hefei	3.80	2.75	-27.68	3.03	0.82
2019	Total	4.44	4.28	-3.53	1.31	0.90
	Shanghai	6.77	6.70	-1.06	1.30	0.85
	Hangzhou	5.93	5.87	-1.12	1.59	0.82
	Nanjing	4.18	3.58	-14.42	1.86	0.84
	Hefei	3.07	3.16	2.74	2.05	0.82
G20	Total	25.84	24.91	-3.61	2.19	0.90
	Shanghai	27.10	25.32	-6.55	2.97	0.72
	Hangzhou	26.48	25.02	-5.51	3.32	0.73
	Nanjing	25.86	24.81	-4.07	2.57	0.76
	Hefei	25.87	25.44	-1.70	2.96	0.80

Table S3. Comprehensive evaluation statistics of the constrained relative humidity over the whole domain as well as in four representative cities as follows: Shanghai, Hangzhou, Nanjing, and Hefei.

Episode	Area	Observations (%)	Constrained Rative humidity (%)	NMB (%)	RMSE (%)	R
2016	Total	75.41	63.95	-15.21	13.25	0.93
	Shanghai	67.89	64.13	-5.53	7.92	0.93
	Hangzhou	78.85	66.72	-15.39	14.44	0.92
	Nanjing	71.58	62.02	-13.31	13.33	0.87
	Hefei	73.47	61.74	-15.96	15.01	0.87
2019	Total	77.62	72.87	-6.12	10.41	0.89
	Shanghai	71.72	77.27	7.74	11.45	0.84
	Hangzhou	77.65	77.79	0.18	12.47	0.81
	Nanjing	74.75	73.54	-1.63	12.22	0.85
	Hefei	80.91	72.82	-10.00	15.15	0.83
G20	Total	65.34	63.97	-2.09	11.21	0.76
	Shanghai	60.67	66.07	8.91	9.83	0.88
	Hangzhou	62.27	62.63	0.57	8.83	0.88
	Nanjing	57.25	60.09	4.95	7.06	0.87
	Hefei	61.13	59.08	-3.36	8.01	0.89

Table S4. Comprehensive evaluation statistics of the constrained wind speed over the whole domain as well as in four representative cities as follows: Shanghai, Hangzhou, Nanjing, and Hefei.

Episode	Area	Observations (m s⁻¹)	Constrained Wind speed (m s⁻¹)	NMB (%)	RMSE (m s⁻¹)	R
2016	Total	2.22	2.62	17.91	0.47	0.98
	Shanghai	0.70	0.73	4.01	0.17	0.99
	Hangzhou	2.27	2.61	15.34	0.55	0.95
	Nanjing	2.40	2.70	12.72	0.46	0.97
	Hefei	1.99	2.33	17.42	0.49	0.96
2019	Total	1.86	2.16	15.85	0.33	0.98
	Shanghai	0.62	0.62	0.25	0.23	0.97
	Hangzhou	1.99	2.10	5.16	0.17	0.99
	Nanjing	2.05	2.30	12.08	0.35	0.97
	Hefei	2.13	2.31	8.35	0.32	0.98
G20	Total	1.96	2.32	18.33	0.41	0.99
	Shanghai	0.51	0.64	26.10	0.14	0.99
	Hangzhou	2.61	2.83	8.64	0.46	0.96
	Nanjing	2.25	2.36	4.73	91.12	0.99
	Hefei	1.82	1.93	6.12	0.23	0.99

Table S5. Comprehensive evaluation statistics of the constrained air pressure over the whole domain as well as in four representative cities as follows: Shanghai, Hangzhou, Nanjing, and Hefei.

Episode	Area	Observations (hPa)	Constrained air pressure (hPa)	NMB (%)	RMSE (hPa)	R
2016	Total	1019.08	1023.50	0.43	4.48	0.99
	Shanghai	1026.53	1029.26	0.27	2.84	0.99
	Hangzhou	1021.98	1024.79	0.28	2.90	0.99
	Nanjing	1023.71	1027.61	0.38	3.94	0.99
	Hefei	1024.72	1028.18	0.34	3.50	0.99
2019	Total	1024.25	1023.27	-0.10	1.17	0.99
	Shanghai	1027.72	1027.73	0.00	0.81	0.98
	Hangzhou	1023.15	1023.21	0.01	0.84	0.99
	Nanjing	1024.63	1026.72	0.20	2.20	0.99
	Hefei	1022.00	1024.36	0.23	2.39	0.99
G20	Total	1003.93	1005.01	0.11	1.09	0.99
	Shanghai	1006.99	1007.54	0.06	0.64	0.99
	Hangzhou	1002.85	1003.52	0.07	0.68	0.99
	Nanjing	1004.13	1005.05	0.09	6.70	0.99
	Hefei	1005.18	1006.84	0.16	1.67	0.99

Table S6. Different effects between the long-term emission controls from 2016 to 2019 and the emergency emission controls during the G20 summit on PM_{2.5}.

Effect	Region	Net impacts	Meteorological impacts	Anthropogenic impacts
		($\mu\text{g}/\text{m}^3$ / %)	($\mu\text{g}/\text{m}^3$ / %)	($\mu\text{g}/\text{m}^3$ / %)
Long-term emission controls	YRD	-2.13/-3.15	11.51/16.21	-13.64/-19.36
	Shanghai	-13.26/-21.22	5.41/17.55	-18.67/-38.77
	Hangzhou	-12.51/-17.18	5.88/19.57	-18.39/-36.75
	Nanjing	-6.32/-8.41	16.51/24.52	-22.83/-32.93
	Hefei	-2.31/-2.71	18.31/20.55	-20.62/-23.26
Emergency emission controls	YRD	-17.23/-41.45	4.83/2.57	-22.06/-44.02
	Shanghai	-11.33/-24.20	9.72/20.95	-20.95/-45.16
	Hangzhou	-21.31/-42.40	2.88/5.76	-24.21/-48.17
	Nanjing	-15.54/-31.51	5.27/10.70	-20.82/-42.21
	Hefei	-12.53/-27.05	5.22/11.27	-17.75/-38.33